



LAWRENCE
LIVERMORE
NATIONAL
LABORATORY

Phosphorescent Heteroleptic Iridium(III) Cyclometallates: Improved Syntheses of Acetylacetonate Complexes and Quantum Chemical Studies of Their Excited State Properties

R. D. Sanner, N. J. Cherepy, H. Q. Pham, V. G.
Young

January 6, 2020

Polyhedron

Disclaimer

This document was prepared as an account of work sponsored by an agency of the United States government. Neither the United States government nor Lawrence Livermore National Security, LLC, nor any of their employees makes any warranty, expressed or implied, or assumes any legal liability or responsibility for the accuracy, completeness, or usefulness of any information, apparatus, product, or process disclosed, or represents that its use would not infringe privately owned rights. Reference herein to any specific commercial product, process, or service by trade name, trademark, manufacturer, or otherwise does not necessarily constitute or imply its endorsement, recommendation, or favoring by the United States government or Lawrence Livermore National Security, LLC. The views and opinions of authors expressed herein do not necessarily state or reflect those of the United States government or Lawrence Livermore National Security, LLC, and shall not be used for advertising or product endorsement purposes.

Phosphorescent Heteroleptic Iridium(III) Cyclometallates: Improved Syntheses of Acetylacetonate Complexes and Quantum Chemical Studies of Their Excited State Properties

Robert D. Sanner,*† Nerine J. Cherepy†, Hung Q. Pham,‡ and Victor G. Young, Jr.‡

†Lawrence Livermore National Laboratory, Livermore, CA 94550, United States

‡Department of Chemistry, University of Minnesota, Minneapolis, MN 55455, United States

ABSTRACT: We have investigated methods to prepare cyclometallated iridium(III) complexes with efficient photoluminescence spanning a broad color palette. In particular, we find that addition of ancillary ligands to chloro-bridged iridium dimers proceeds cleanly in refluxing 1,2-dimethoxyethane (DME) without the need for additional product purification. This represents an improvement over the conventional use of 2-ethoxyethanol which requires column chromatographic separation. Our efforts in this work have focused on acetylacetonate complexes such as $(F_2ppy)_2Ir(acac)$, where $F_2ppy = 2-(4',6'-difluorophenyl)pyridinato$. We have prepared fifteen compounds by the route, eight of which are newly reported; in four cases we were able to prepare complexes which were inaccessible via the conventional route. Nine of the complexes were characterized by single crystal x-ray diffraction and possess the same distorted octahedral geometry around the iridium with two bidentate phenylpyridine ligands and one bidentate acetylacetonate ligand. Seven of the complexes exhibited efficient photoluminescence with colors ranging from yellow to blue and quantum yields of 0.51-0.74. All of the compounds with trifluoromethyl or phenyl substituents on the acetylacetonate displayed emission in the orange with low quantum efficiency. The use of TD-DFT calculations, along with natural transition orbitals (NTOs), permitted a detailed interpretation of the electronic structures for the complexes. The nature of the acceptor orbitals for the low energy triplet state NTOs proved to be an important predictor for the emission spectra of the compounds.

Keywords:

Photoluminescence

Phosphorescent iridium complex

DFT calculations

OLED

Cyclometallated iridium synthesis

INTRODUCTION

Phosphorescent cyclometallated iridium(III) compounds have been widely studied for diverse applications such as solar cells,¹⁻⁶ sensors,⁷⁻¹⁰ bioimaging,¹¹⁻¹³ and scintillators.¹⁴⁻¹⁸ Their electrophosphorescence, in which light emission is triggered by an electric charge, has also prompted research in the areas of light-emitting electrochemical cells,¹⁹⁻²² electrogenerated chemiluminescence,²³⁻²⁶ and organic light-emitting diodes (OLED's).²⁷⁻³⁶ The strong spin-orbit coupling engendered by the iridium atom allows for the mixing of singlet and triplet excited states through efficient intersystem crossing.³⁷⁻⁴⁰ Phosphorescence quantum yields are thus increased beyond that obtainable with solely fluorescent emitters.⁴¹ These cyclometallated iridium(III) complexes may be classified based on their associated ligands. Thus, homoleptic compounds such as Ir(ppy)₃⁴² (where ppy = 2-phenylpyridinato) or Ir(F₂ppy)₃⁴³ (where F₂ppy = 2-(4',6'-difluorophenyl)pyridinato) possess identical ligands. These are differentiated from heteroleptic compounds such as (F₂ppy)₂Ir(pic)⁴⁴ (where pic = picolate or pyridine-2-carboxylate) or (F₂ppy)(ppy)Ir(acac)⁴⁵ (where acac = acetylacetonate) that contain at least two different ligands. The cyclometallated ligands, for instance phenylpyridine, typically contain a (C^N) core and are distinguished from the ancillary ligands such as picolate or acetylacetonate. Although (F₂ppy)₂Ir(pic), commonly referred to as FIrpic, has received the most study of the heteroleptic compounds,^{44, 46} the class of complexes containing acetylacetonate as the ancillary ligand has also been a fertile area of research. Since early reports of (ppy)₂Ir(acac)⁴² and (F₂ppy)₂Ir(acac), also known as FIracac,⁴⁷ an assortment of substituted β-diketonates have appeared. They have been the subject of spectroscopic³⁸ and theoretical⁴⁸⁻⁵¹ studies. The synthesis of these complexes typically involves a two-step process. First, the cyclometallating ligand is reacted with IrCl₃ · x H₂O following the example of Nonoyama⁵² or Sprouse⁵³ to form a chloro-bridged dimeric iridium compound, *e.g.* [(ppy)₂IrCl]₂.^{53, 54} Next, the ancillary ligand is added by reacting the iridium dimer with acetylacetone in refluxing 2-ethoxyethanol and base (usually Na₂CO₃).^{23, 47, 55, 56} In a variation, Baranoff⁴⁵ has used tetrabutylammonium hydroxide as base in refluxing dichloromethane. After the second step it is necessary to perform additional purification, usually concluding with column chromatography. As part of our synthesis program for plastic scintillators^{17, 57} we have investigated iridium complexes that emit in the deep blue.⁵⁸ We have now expanded our spectral range to include longer wavelength emitters, concentrating on heteroleptic iridium(III) (bis)cyclometallates. This effort has led us to report an improved synthesis of FIrpic and other picolines:⁵⁹ We found that refluxing 1,2-dimethoxyethane in the presence of sodium carbonate made an excellent reaction medium for addition of the ancillary picolate ligand to the chloro-bridged iridium dimer. Furthermore, we were able to obtain yields equal to or better than those reported in prior procedures without the need for time-consuming purification steps (such as column chromatography). We have now broadened the scope of this reaction by the investigation of acetylacetonates as the ancillary ligand and report those results herein. The products were characterized by NMR and optical spectroscopy, x-ray crystallography, and photophysical measurements. Time-

dependent density functional theory (TD-DFT) calculations were performed on the complexes with the goal of interpretation of their absorption and emission spectra.

RESULTS AND DISCUSSION

Synthesis. The reaction to prepare heteroleptic iridium complexes $(X_2ppy)_2Ir(acac-R_i)$ using 1,2-dimethoxyethane at reflux with base is shown in Scheme 1, where $X = H$ or F and R_i are various substituents on the acetylacetonate ligand, including methyl, trifluoromethyl, cyclopentyl, cyclohexyl, and phenyl. Reaction times are typically 6-8 hr and workup consists of simple filtration and washing; yields range from 76-92% except in two cases (**2** and **13**) which will be discussed below. An identification guide to compounds **1-15** prepared in this work is given in Chart 1.

Scheme 1. Synthesis of iridium(III) acetylacetonate complexes.

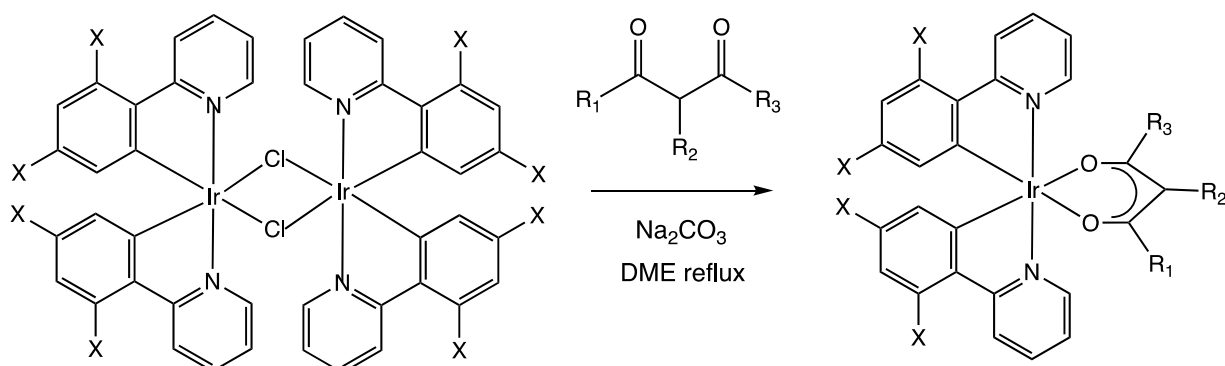
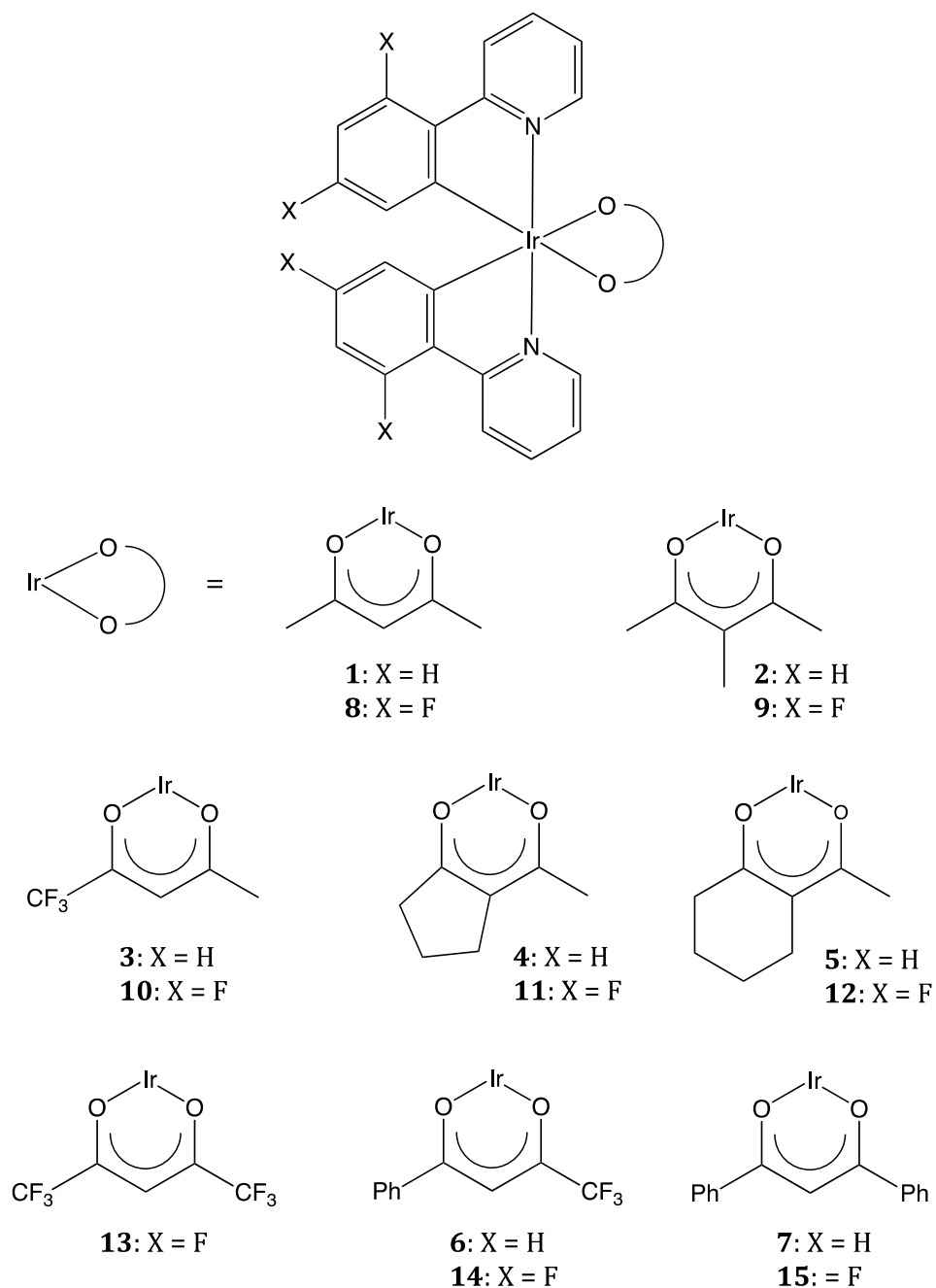


Chart 1. Heteroleptic iridium(III) acetylacetonates prepared in this study.



Compounds **1-7** employed $[(ppy)_2IrCl]_2$ ^{53, 54} as the iridium source while **8-15** used $[(F_2ppy)_2IrCl]_2$.^{47, 60} Compounds **1**,^{42, 45} **2**,⁶¹ **4**,⁶¹ **5**,⁶¹ **7**,⁵⁴ **8**,^{44, 45, 47, 62} **9**,⁶³ and **15**^{55, 64} have been previously prepared, usually by mixing the iridium dimer with an acetylacetonate derivative in refluxing 2-ethoxyethanol and base; purification is accomplished by column chromatography. In our reactions, column chromatography was only required in the case of compound **13**.

An NMR comparison of the Flracac obtained for 12 hr reactions by our DME method and the ethoxyethanol method is shown in Fig. 1 (^1H , aromatic region). Note the higher purity of the crude product obtained in DME as demonstrated in the bottom trace of the ^1H NMR spectra. We believe that the gentler conditions of DME

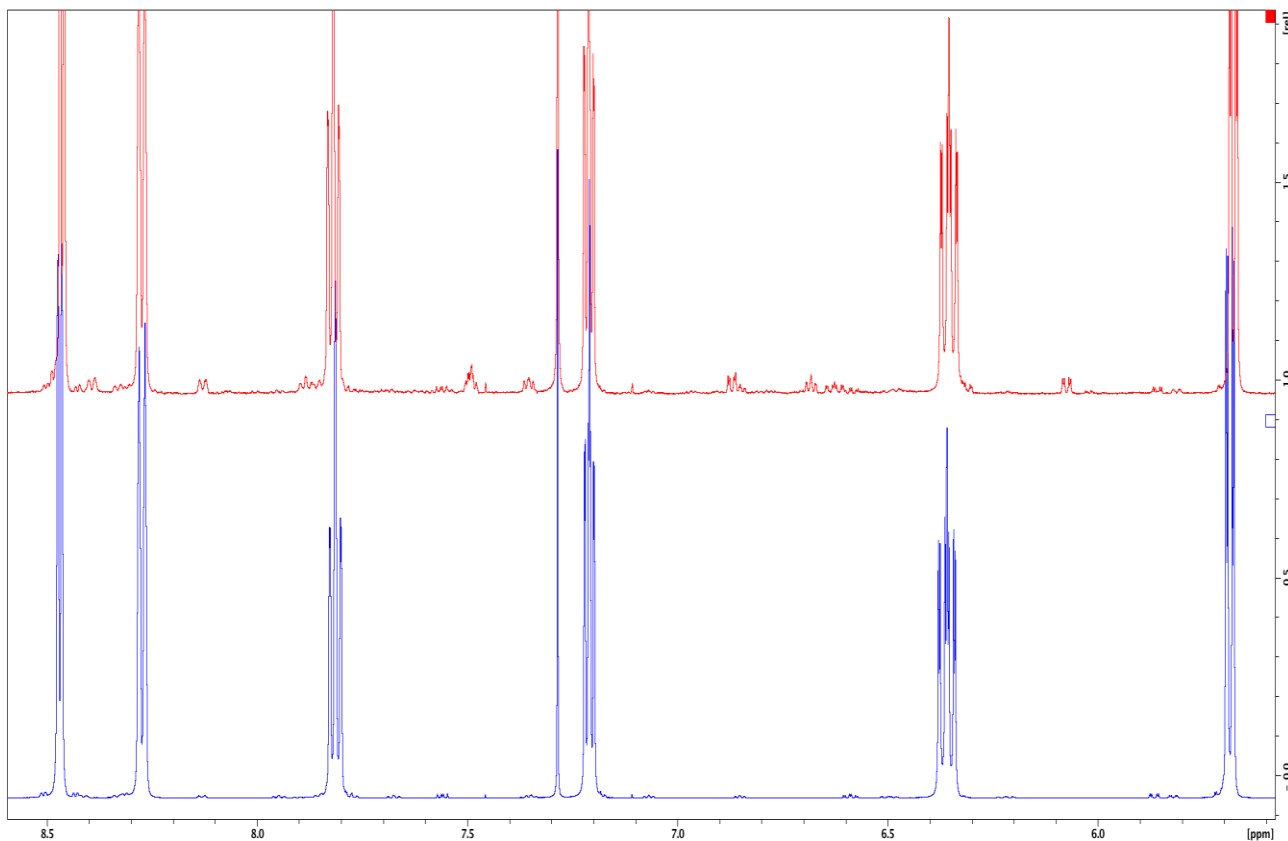


Figure 1. ^1H NMR spectra of crude Flracac prepared in ethoxyethanol (top) and dimethoxyethane (bottom).

reflux (85° C) compared to ethoxyethanol (134°) are at least partly responsible for this difference. Our method did not result in any loss in yield as all starting material was consumed and the desired product was cleanly obtained. We have found that this reaction proceeds smoothly with both $(\text{ppy})_2\text{Ir}$ and $(\text{F}_2\text{ppy})_2\text{Ir}$ moieties and most acetylacetonate derivatives we examined. Although we have only performed this with a maximum 2 g of iridium starting material, scale-up should not be a problem. In fact, the ability to omit column chromatography would be most useful at larger scales.

A few cases deserve special mention. The diketonate ligand that contains two trifluoromethyl groups, hexafluoroacetylacetonate, was unreactive with $[(\text{ppy})_2\text{IrCl}]_2$ in either refluxing DME or methoxyethanol; starting materials were recovered unchanged. The reaction of this ligand with $[(\text{F}_2\text{ppy})_2\text{IrCl}]_2$ to form **13** did occur but was very slow: after 24 hr reflux there was still ~20% iridium starting material left as well as ~10% impurity. The product was successfully isolated using column chromatography and Soxhlet extraction but with only 40% yield. Attempts to prepare **13** in refluxing methoxyethanol were unsuccessful:

although a product was cleanly formed that contained the $(F_2ppy)_2Ir$ moiety, ^{19}F NMR showed there were no CF_3 groups present. Both acetylacetonate ligands that we examined containing one trifluoromethyl group, 1,1,1-trifluoro-2,4-pentanedione and 4,4,4-trifluoro-1-phenyl-1,3-butanedione, reacted swiftly and cleanly with $[(ppy)_2IrCl]_2$ and $[(F_2ppy)_2IrCl]_2$ to form **3**, **6**, **10**, and **14**. It is noteworthy that using the glycol ether route with refluxing ethoxyethanol gave only non-emissive products in attempts to prepare **10** and **14**, proving the superiority of the DME route. The ligand 2-acetylcyclohexanone required much longer reaction times with $[(ppy)_2IrCl]_2$ (24 hr) than with $[(F_2ppy)_2IrCl]_2$ (6 hr) to go to completion, forming **5** and **12**, respectively. We also attempted to prepare **5** in refluxing ethoxyethanol, and an NMR comparison of the crude products obtained for the DME and ethoxyethanol reactions is illustrated in Fig. 2. Again, as shown for FIracac in Fig. 1,

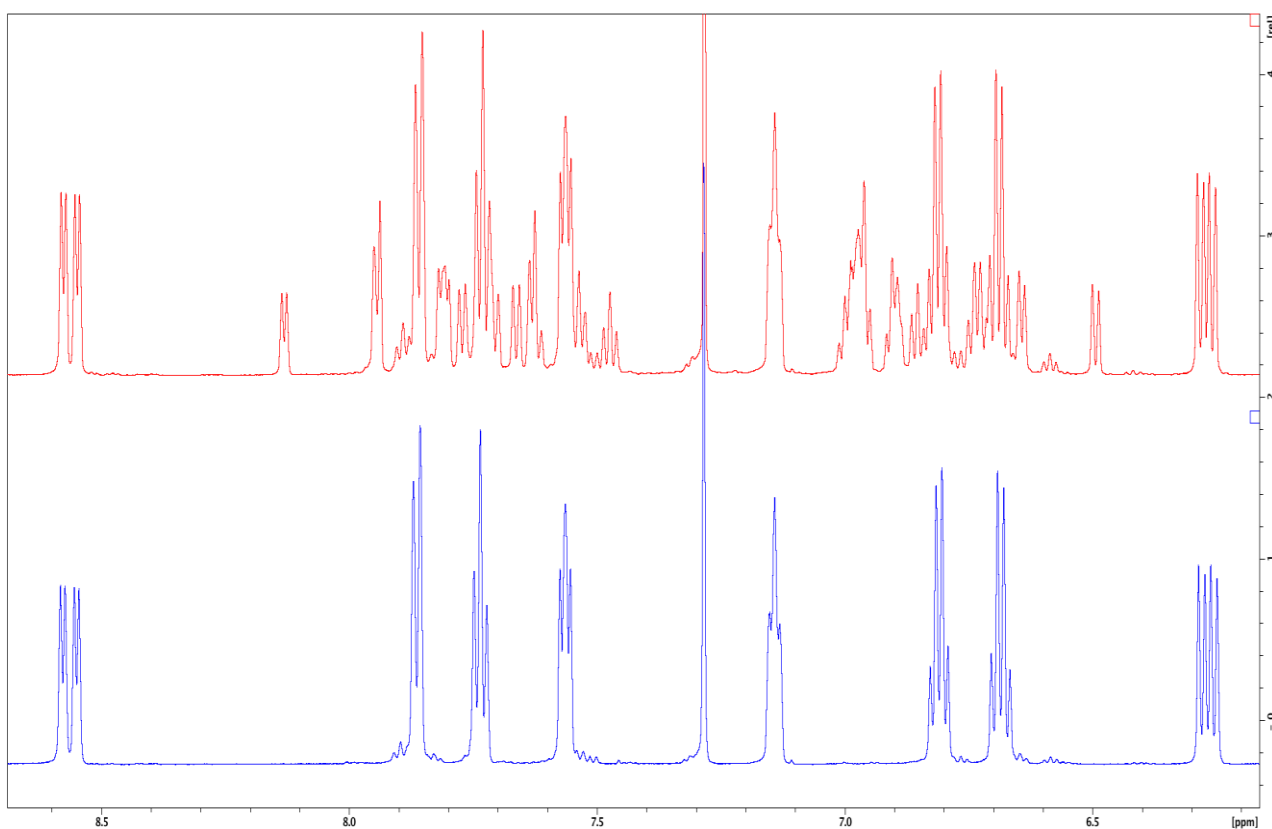


Figure 2. 1H NMR spectra of crude compound **5** prepared in ethoxyethanol (top) and dimethoxyethane (bottom).

DME provided a much cleaner product than ethoxyethanol. The 2-acetylcyclopentanone ligand did not show the disparity in reaction rates between $[(ppy)_2IrCl]_2$ and $[(F_2ppy)_2IrCl]_2$ that was found with its cyclohexanone analog since **4** and **11** both exhibited facile formation in 6 hr at DME reflux. Finally, 3-methylacetylacetonate reacted quickly with $[(F_2ppy)_2IrCl]_2$ to form **9** but slowly with $[(ppy)_2IrCl]_2$ to form **2**: 24 hr was required to consume all iridium starting material with concomitant formation of the desired product and an unidentified compound that proved difficult to separate. The attempt to form **2** in ethoxyethanol was much less successful, as none of the desired product was formed in 24 hr. The previous

report⁶¹ of compound **2** shows NMR results that are at variance with ours (see Experimental).

Crystal Structure Determinations. The molecular structure of compounds **3**, **5**, **6**, and **9-14** have been confirmed by X-ray crystallography and ORTEP diagrams of these complexes are shown in Figs. 3-11; crystal and structure refinement data are provided in Supporting Information (Tables S1-S9). All the complexes exhibit the same distorted octahedral geometry with two bidentate phenylpyridine ligands (coordinated through the pyridine nitrogen atom and a phenyl carbon atom) and one bidentate 2,4-pentanedionate framework ligand (coordinated through the diketonate oxygen atoms). The iridium-bound nitrogen atoms of the phenylpyridine ligands are *trans* to each other while the phenyl carbon atoms bound to the iridium are *cis*. The two ligated oxygen atoms in the β -diketonate ligand are then *trans* to the phenyl carbon atoms of the phenylpyridine ligand. The Ir-N and Ir-C distances for the phenylpyridine ligand are remarkably consistent throughout these molecules, averaging 2.036(8) Å and 1.992(11) Å, respectively. The Ir-O distances for the β -diketonate ligand within a molecule are nearly equal and this distance varies as expected among the various diketonates. Thus, the ligands with electron-withdrawing CF₃ groups show the longest Ir-O bond lengths (e.g. 2.18 Å for **3**) while those without these groups show shorter bonds (e.g. 2.11 Å for **9** and **12**). The ligands with both a phenyl and a CF₃ group fall midway between these extremes (2.14 Å for **6** and **14**). The Ir-O distance averaged over all the complexes is 2.14 Å. This is an elongation of the mean value of 2.088 Å reported in the Cambridge Crystallographic Database⁶⁵ for an Ir-O bond, illustrating the *trans* effect of the phenyl group in the phenylpyridine ligand for these molecules. The C-Ir-N “bite” angle for the phenylpyridine ligands is consistent, averaging 81.0(3)° for these complexes. As expected, there is more variation in the O-Ir-O angle for the collection of diketonate ligands investigated, ranging from 84.76(7)° for the acetylcylohexanone ligand in **5** to 90.0(1)° in the acetylcylopentanone complex **11**; the average for this angle over all the complexes is 87.7°. The phenyl and pyridine rings in each phenylpyridine ligand are slightly twisted with respect to each other across the C-C bond linking the two rings. The dihedral angle between best planes for the two rings is typically in the range of 3°- 6°, although **6** shows a larger twist angle of 10.1° for one of the ligands. Examination of a packing diagram for **6** shows close intermolecular contacts between a chlorine atom on the dichloromethane solvate molecule and two carbon atoms on the pyridine ring.

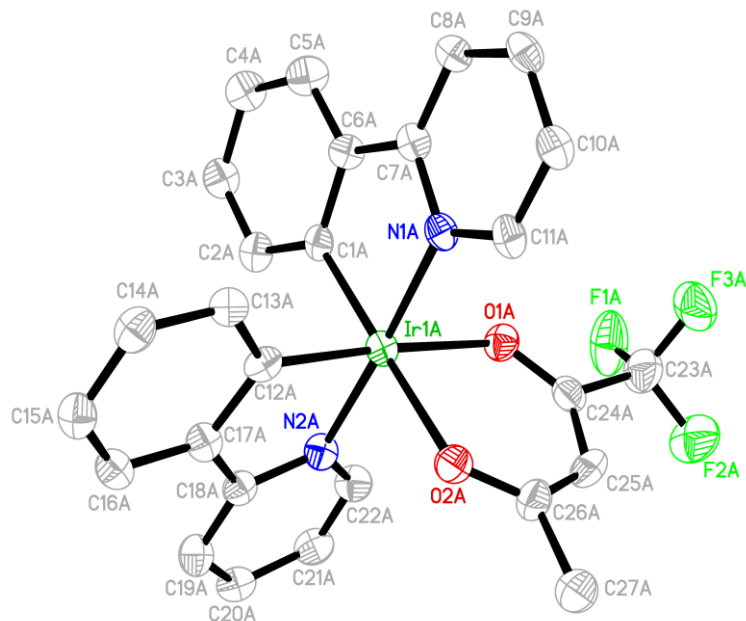


Figure 3. The molecular structure of compound **3a**, with atom labeling and displacement ellipsoids drawn at the 50% probability level. Hydrogen atoms have been removed for clarity. Two molecules are found in the asymmetric unit; only molecule A is shown in the figure. Only one component of the disordered trifluoropentanedionate ligand pair is shown. Selected bond distances (Å) and angles (°): Ir1A-C1A 2.030(9), Ir1A-C12A 1.983(9), Ir1A-N1A 2.048(7), Ir1A-N2A 2.027(8), Ir1A-O1A 2.177(6), Ir1A-O2A 2.183(6), C1A-Ir1A-N1A 81.0(3), C12A-Ir1A-N2A 80.9 (3), O1A-Ir1A-O2A 88.3(2).

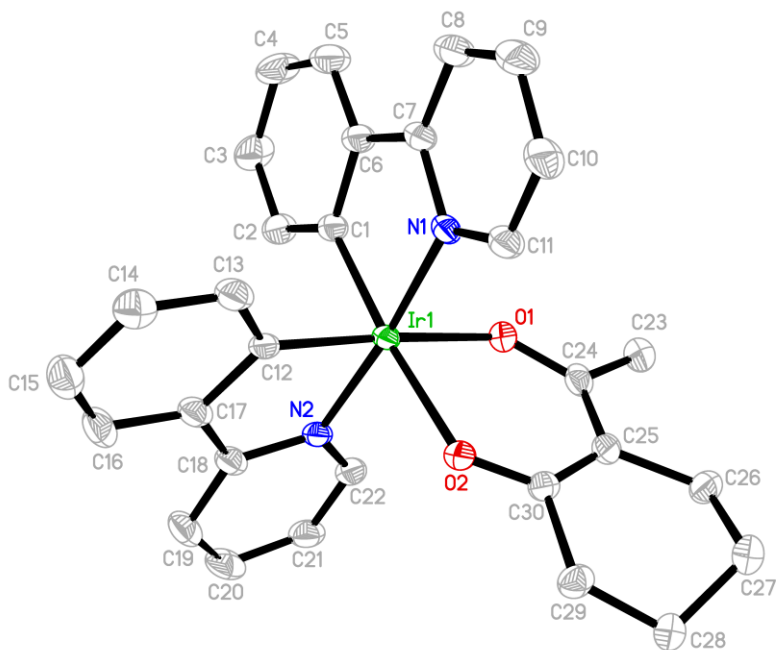


Figure 4. The molecular structure of compound **5**, with atom labeling and displacement ellipsoids drawn at the 50% probability level. Hydrogen atoms and dichloromethane solvent have been omitted for clarity. Only one component of the disordered acetylcyclohexanoate ligand pair is shown. Selected bond distances (Å) and angles (°): Ir1-C1 2.001(3), Ir1-C12 1.990(3), Ir1-N1 2.028(2), Ir1-N2 2.041(2), Ir1-O1 2.142(2), Ir1-O2 2.147(2), C1-Ir1-N1 80.74(10), C12-Ir1-N2 80.88(10), O1-Ir1-O2 84.76(7).

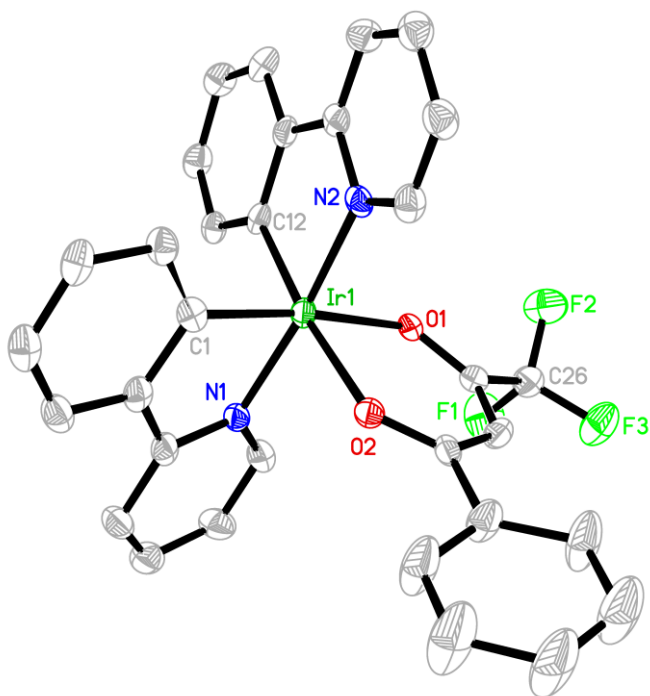


Figure 5. The molecular structure of compound **6**, with atom labeling and displacement ellipsoids drawn at the 50% probability level. Hydrogen atoms and dichloromethane solvent have been omitted for clarity. Selected bond distances (Å) and angles (°): Ir1-C1 1.986(8), Ir1-C12 1.986(9), Ir1-N1 2.054(8), Ir1-N2 2.043(8), Ir1-O1 2.151(5), Ir1-O2 2.138(7), C1-Ir1-N1 80.2(4), C12-Ir1-N2 80.5(4), O1-Ir1-O2 88.1(3).

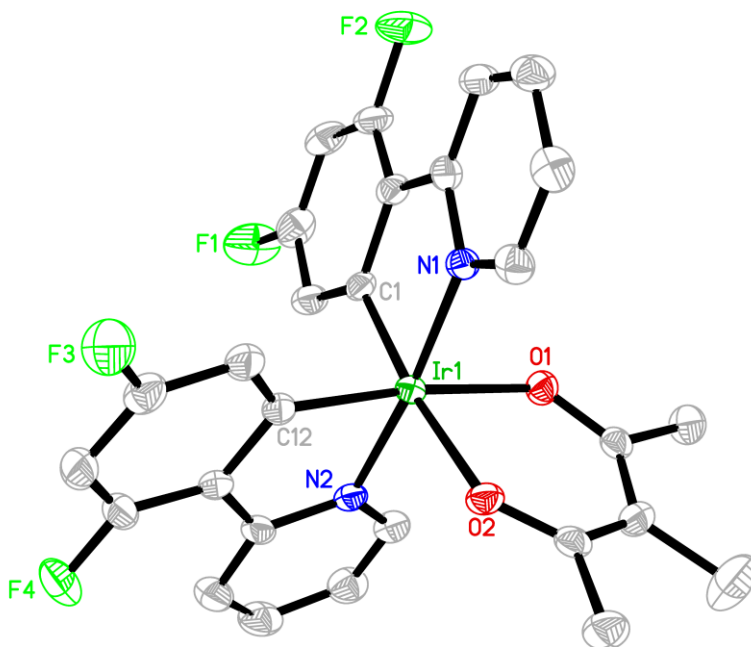


Figure 6. The molecular structure of compound **9**, with atom labeling and displacement ellipsoids drawn at the 50% probability level. Hydrogen atoms have been removed for clarity. Selected bond distances (Å) and angles (°): Ir1-C1 1.987(3), Ir1-C12 1.994(3), Ir1-N1 2.036(2), Ir1-N2 2.035(2), Ir1-O1 2.108(2), Ir1-O2 2.120(2), C1-Ir1-N1 81.08(10), C12-Ir1-N2 81.05(10), O1-Ir1-O2 86.58(7).

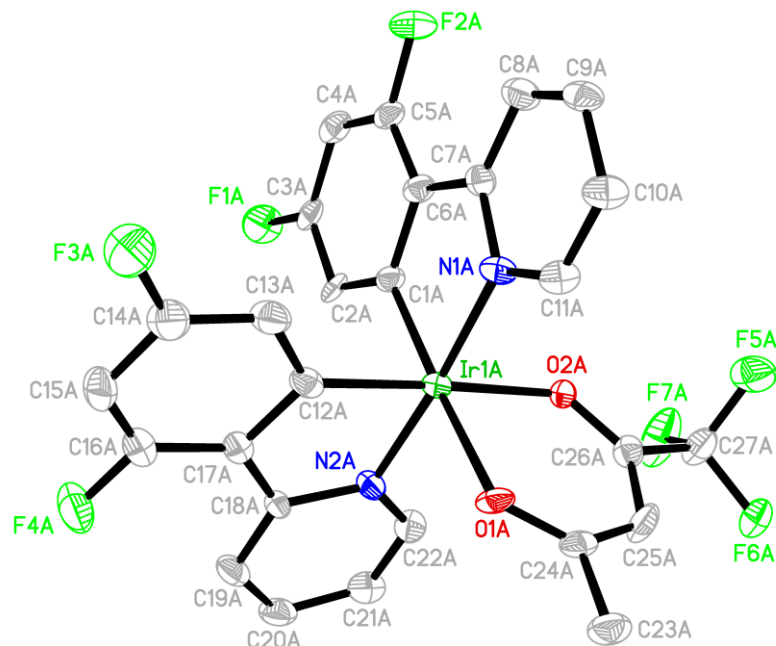


Figure 7. The molecular structure of compound **10a**, with atom labeling and displacement ellipsoids drawn at the 50% probability level. Hydrogen atoms have been removed for clarity. Two molecules are found in the asymmetric unit; only molecule A is shown in the figure. Only one component of the disordered trifluoropentanedionate ligand pair is shown. Selected bond distances (Å) and angles (°): Ir1A-C1A 1.988(10), Ir1A-C12A 1.976(10), Ir1A-N1A 2.040(8), Ir1A-N2A 2.038 (7), Ir1A-O1A 2.165(7), Ir1A-O2A 2.117(7), C1A-Ir1A-N1A 80.4(4), C12A-Ir1A-N2A 81.0 (4), O1A-Ir1A-O2A 87.9(2).

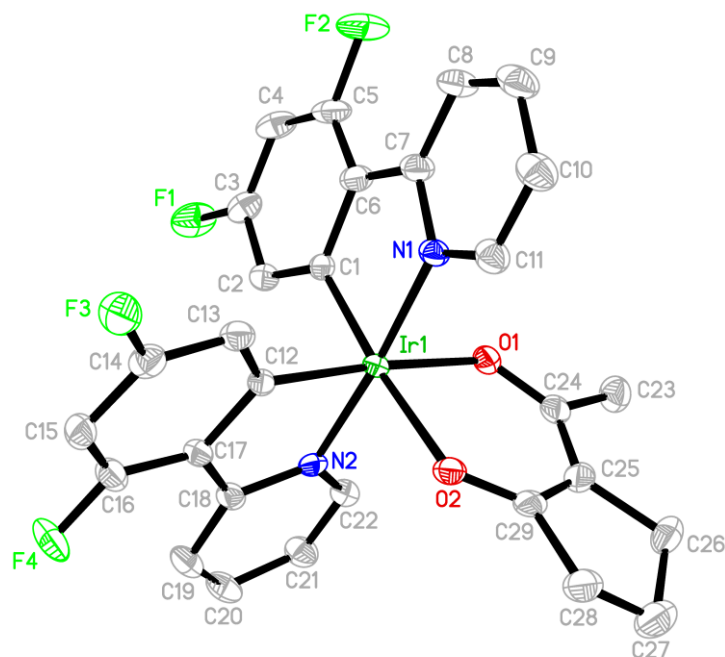


Figure 8. The molecular structure of compound **11**, with atom labeling and displacement ellipsoids drawn at the 50% probability level. Hydrogen atoms have been removed for clarity. Selected bond distances (Å) and angles (°): Ir1-C1 1.989(3), Ir1-C12 1.991(3), Ir1-N1 2.030(3), Ir1-N2 2.030(3), Ir1-O1 2.130 (3), Ir1-O2 2.134(2), C1-Ir1-N1 81.26(13), C12-Ir1-N2 81.09(13), O1-Ir1-O2 89.97(10).

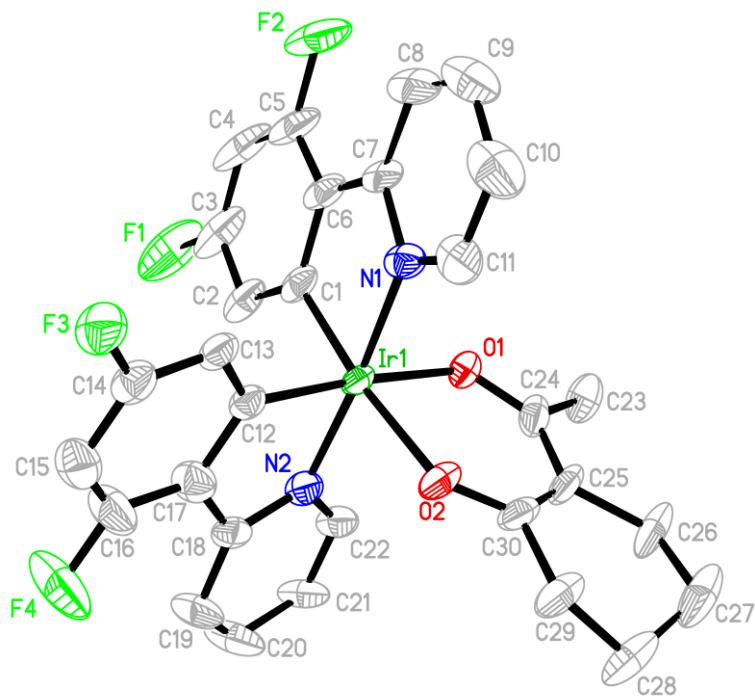


Figure 9. The molecular structure of compound **12**, with atom labeling and displacement ellipsoids drawn at the 50% probability level. Hydrogen atoms have been removed for clarity. Only one component of the disordered whole molecule pair is shown. Selected bond distances (Å) and angles (°): Ir1-C1 1.984(6), Ir1-C12 1.993(7), Ir1-N1 2.032(6), Ir1-N2 2.035(6), Ir1-O1 2.105(6), Ir1-O2 2.125(6), C1-Ir1-N1 81.3(3), C12-Ir1-N2 81.0(4), O1-Ir1-O2 86.1(3).

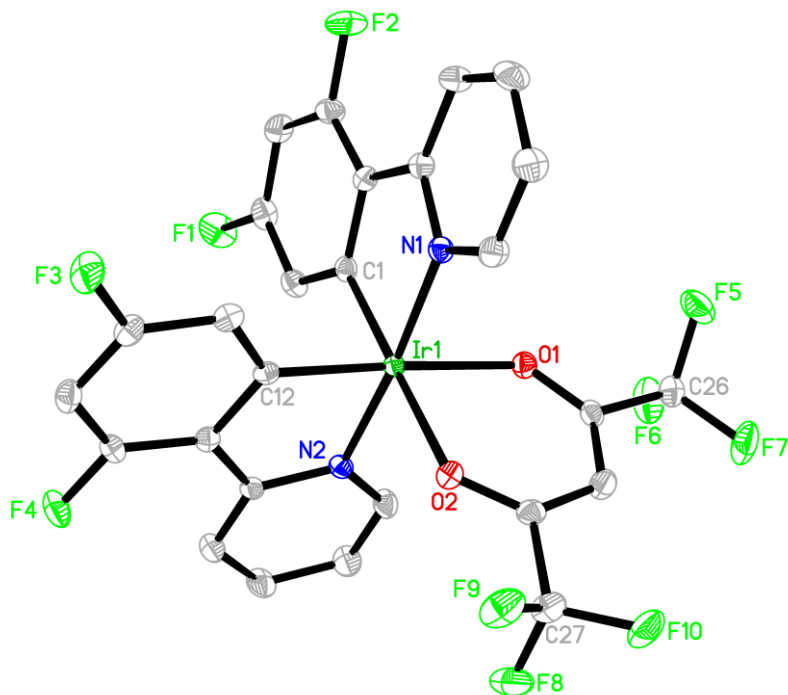


Figure 10. The molecular structure of compound **13**, with atom labeling and displacement ellipsoids drawn at the 50% probability level. Hydrogen atoms have been removed for clarity. Selected bond distances (Å) and angles (°): Ir1-C1 1.985(2), Ir1-C12 1.983(2), Ir1-N1 2.039(2), Ir1-N2 2.035(2), Ir1-O1 2.156(2), Ir1-O2 2.158(2), C1-Ir1-N1 80.60(8), C12-Ir1-N2 81.01(8), O1-Ir1-O2 87.57(6).

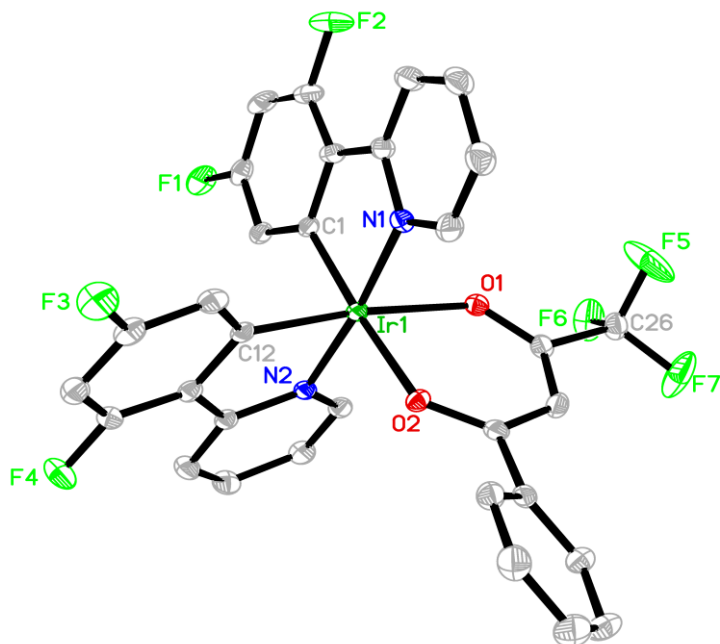


Figure 11. The molecular structure of compound **14**, with atom labeling and displacement ellipsoids drawn at the 50% probability level. Hydrogen atoms and dichloromethane solvent have been omitted for clarity. Selected bond distances (Å) and angles (°): Ir1-C1 1.985(2), Ir1-C12 1.988(2), Ir1-N1 2.039(2), Ir1-N2 2.036(2), Ir1-O1 2.151(2), Ir1-O2 2.122(2), C1-Ir1-N1 80.98(9), C12-Ir1-N2 80.91(9), O1-Ir1-O2 87.92(6).

The molecular structures of all the complexes were successfully solved, although there were special features of some, which will now be discussed.

Compound 3. The crystal was a twin by non-merohedry and the masses of the twin individuals refined to 0.56:0.44. An uncharacteristically long detector distance of 16 cm was required to better separate streaky reflections caused by the twinning. Data completion was >95% for these conditions while shorter detector distances led to greater data losses. The twin law corresponds to a rotation of 180° about the (111) reciprocal axis (see CIF file for the matrix used to convert *hkl* data). The 1,1,1-trifluoro-2,4-pentanedionate ligand is disordered across a pseudo-twofold axis that passes through the iridium atom and the carbon at the 3-position in the pentanedionate ligand (C25 in Fig. 3); this flips the positions of the methyl and trifluoromethyl groups in the disordered pair. The asymmetric unit for the structure has two molecules ($Z'=2$) that exist as an enantiomeric pair (A and B) and the disordered ligand exists in ratios of 0.69:0.31 in molecule A and 0.76:0.24 in molecule B. Reasonable constraints and restraints for the disordered ligand were applied during refinement (see Supporting Information for details).

Compound 5. The 2-acetylcyclohexanone ligand is disordered in a 0.62:0.38 ratio across a pseudo-mirror plane that is perpendicular to the β -diketonate plane and passes through the iridium atom and the carbon in the 2-position in the 2-acetylcyclohexanone ring (atom C25 in Fig. 4). There is a dichloromethane solvent molecule near the disordered ligand and this proximity causes the solvent to have positional disorder as well. Both disorders were linked with a single occupancy free variable to have the same ratio. Reasonable constraints and restraints for the disordered ligand were applied during refinement (see Supporting Information for details). The conformation of the six-membered ring in the 2-acetylcyclohexanone ligand is worth noting. Cyclohexene is normally found in the “half-chair” conformation in which the two allylic carbons and the two unsaturated carbons are coplanar while the two remaining ring carbon atoms are situated one above and one below this plane.^{66, 67} That is the geometry found in this structure. The ring plane is defined as C25/C26/C29/C30 (or its disordered partner C25'/C26'/C29'/C30'); the average displacement of C27/C27' is -0.50 Å and C28/C28' is +0.28 Å.

Compound 6. The crystal structure is a 1:1 solvate with dichloromethane; the solvent is disordered in overlapping positions in a 4:1 ratio (Fig. S4). The specimen was extremely thin (approx. 1 μm) which necessitated longer than normal 45 second exposures and higher than expected $R_{\text{int}} = 0.064$. Examination of the 4,4,4-trifluoro-1-phenyl-1,3-butanedionate ligand shows the plane of the phenyl group is rotated at an angle of 25.3(6)° out of the diketonate plane.

Compound 9. The crystal structure of the nonfluorinated ring analog, (ppy)₂Ir(3-methylacetylacetonate) (our compound **2**) has been previously reported.⁶⁸ The configuration of the diketonate ligand is similar in both **2** and **9**.

Compound 10. The crystal was a twin by non-merohedry and the masses of the twin individuals refined to 0.53:0.47. The twin law corresponds to a rotation of 180° about the crystallographic a^* axis (see CIF file for the matrix used to convert *hkl* data). There are two molecules in the asymmetric unit, A and B, related to each other by a pseudo-inversion center at approx. (0.497, 0.248, 0.369). The 1,1,1-

trifluoro-2,4-pentanedionate ligand is disordered across a pseudo-twofold axis that passes through the iridium atom and the carbon at the 3-position in the pentanedionate ligand (C25 in Fig. 7); this flips the positions of the methyl and trifluoromethyl groups in the disordered pair. This disordered ligand exists in ratios of 0.75:0.25 in molecule A and 0.85:0.15 in molecule B. Reasonable constraints and restraints for the disordered ligand were applied during refinement (see Supporting Information for details).

Compound 11. The five-carbon ring in the β -diketonate ligand shows a puckered structure. Thus, if we calculate the plane of the two allylic carbons and the two unsaturated carbons (C26/C28/C25/C29 in Fig. 8), it is found that C27 is displaced by 0.373(6) Å from the plane. This conformation is typically found for the carbon atom opposite the double bond in cyclopentene and its derivatives.^{67, 69} We note that the crystal structure of the nonfluorinated ring analog, (ppy)₂Ir(2-acetylcyclopentanone) (our compound **4**) has been previously reported.⁷⁰ This structure displays a disordered diketonate ligand and dichloromethane solvate while our structure of the fluorinated ring analog does not show any disorder or solvated molecules.

Compound 12. This compound was found to be isostructural with **11**. While **11** is well behaved and shows no signs of disorder, **12** exhibits what is best described as whole-molecule disorder. Early results at 173K suggested that cooling to a lower temperature could remove the disorder but collection at 100K did not help. Two complete, partially occupied molecules were refined to a 0.64:0.36 ratio; some disordered pairs of atoms nearly overlap (Fig.S9). Reasonable constraints and restraints were applied during refinement (see Supporting Information for details). Close examination of the six-membered ring in the β -diketonate ligand in Figure 9 shows it to exist in the “half-chair” conformation as was found in compound **5**. The ring plane is defined as C25/C26/C29/C30 (or its disordered partner C25'/C26'/C29'/C30'); the average displacement of C27/C27' is -0.32 Å and C28/C28' is +0.41 Å.

Compound 14. The structure exists as a 1:1 solvate with dichloromethane. It was found that the plane of the phenyl group is rotated 33.8(1)° out of the plane of the diketonate ligand.

Spectroscopy and Photophysical Properties. The absorption spectra above 350 nm of complexes **3-6** in the (ppy)₂Ir(acac) series are shown in the left half of Fig. 12 (complete spectra in Fig. S12 in Supporting Information). In addition

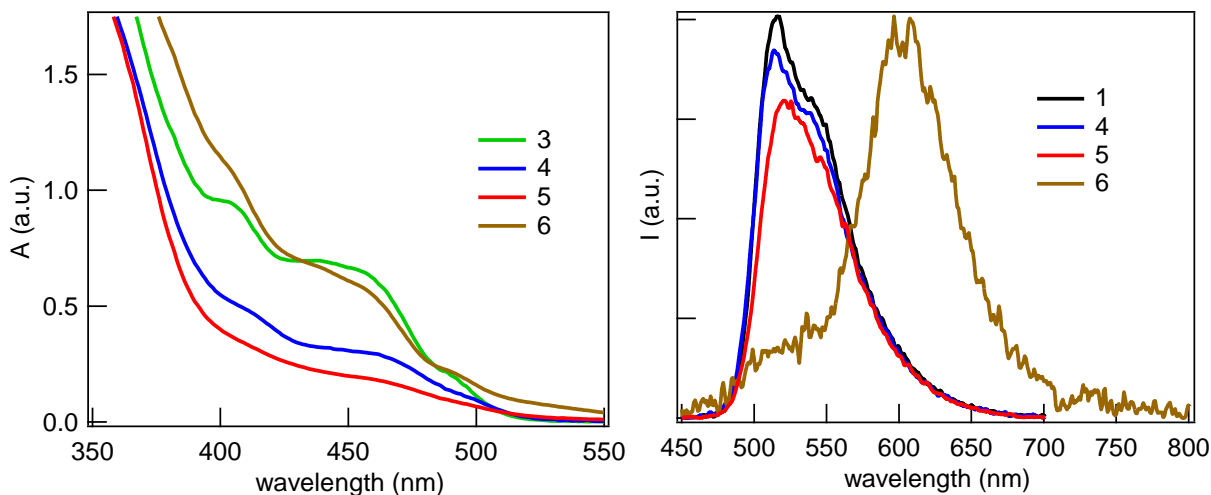


Figure 12. Absorption (left) and emission (right) spectra of (ppy)₂Ir(acac) series (0.1 wt% in PMMA discs).

to intense ligand-centered π - π^* transitions below 375 nm, the common spectral features are a band \sim 400 nm typically assigned as ¹MLCT ($d \rightarrow \pi^*$), a band near 450 nm assigned as mixed singlet and triplet MLCT, and a much weaker absorption at 490 nm usually assigned to ³MLCT between the singlet ground state and the lowest triplet excited state ($S_0 \rightarrow T_1$).^{42, 51, 71} The emission spectra of **1**, **4-6** are given in the right half of Fig. 12 (compound **3** is omitted due to its extremely weak emission). Compounds **1**, **4**, and **5** show a band at approx. 515 nm with a shoulder at longer wavelength (\sim 540 nm) leading to yellow-green emission. Compound **6** exhibits a broad, weak band that is centered near 600 nm, red-shifted \sim 90 nm from the other compounds giving rise to weak orange emission.

The absorption spectra of complexes **9-14** in the FIracac series are shown in Fig. 13 (left). As above for the (ppy)₂Ir(acac) series, the compounds display three bands in addition to the intense ligand-centered π - π^* transition below 350 nm.

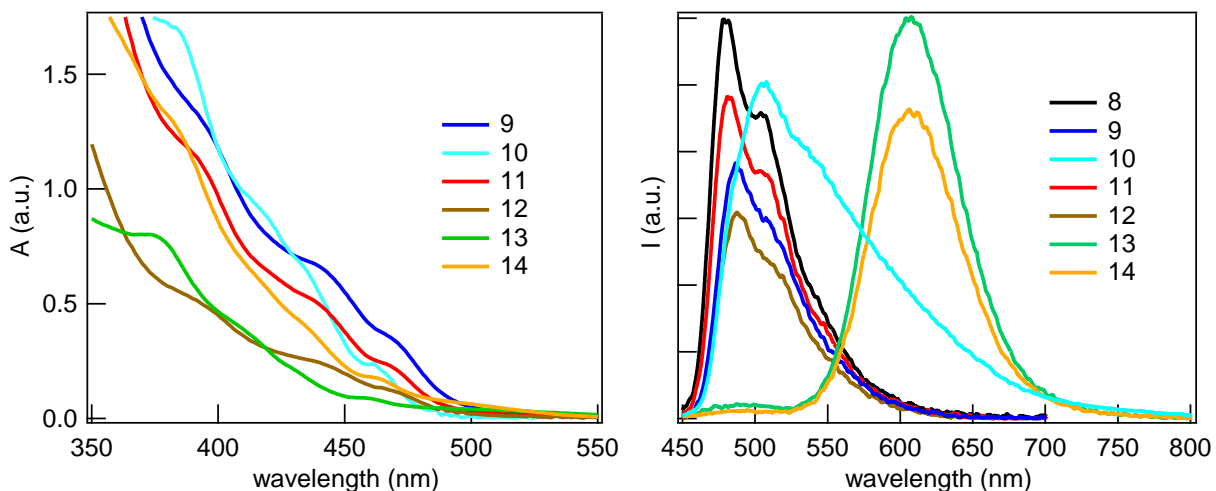


Figure 13. Absorption (left) and emission (right) spectra of FIracac series (0.1 wt% in PMMA discs).

These occur in the spectral regions of 385 nm, 440 nm, and 465 nm. The weakest absorption (465 nm) is blue-shifted \sim 25 nm from the (ppy)₂Ir(acac) series. The emission spectra of **8-14** are given in the right half of Fig. 13 and show more variation than the absorption spectra for the series. In general, the emission bands of the FIracac series are blue-shifted about 35 nm compared to the (ppy)₂Ir(acac) series. Compounds **8**, **9**, **11**, and **12** are nearly identical, with the main band at 480 nm and a shoulder at 505 nm leading to greenish blue emission. Compounds **13** and **14** exhibit weak, broad emission that is centered \sim 610 nm, appearing as an orange color. This is the same behavior shown by **6** from the (ppy)₂Ir(acac) series above. Compound **10** shares characteristics with both of the aforementioned groups. Thus, it has a peak at 506 nm with a shoulder \sim 540 nm giving its spectrum an appearance similar to the **8**, **9**, **11**, **12** group (although red-shifted by 25 nm). It also exhibits the weak emission and band broadening of the **13**, **14** group. It should be noted that all the compounds with weak emission (**3**, **6**, **10**, **13**, **14**) contain at least one CF₃ group. Several of the emissive compounds prepared in this work are shown in Fig. 14.

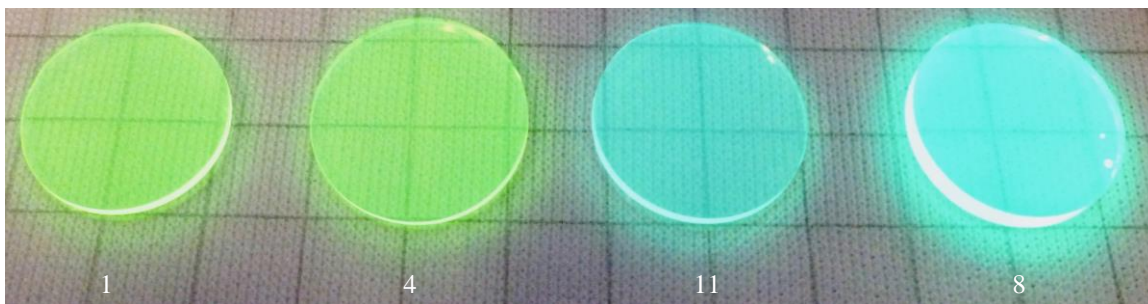


Figure 14. Representative emissive compounds (0.1% in PMMA discs) under 400 nm illumination.

The photophysical properties of the complexes are given in Table 1. In general, the F₂ppy complexes exhibit higher emission quantum yields than their ppy analogs, *e.g.* FIracac > (ppy)₂Ir(acac), although the differences are fairly small. The 2-acetylcyclohexanonate complexes are very emissive; the complex **5** has the highest quantum efficiency in the (ppy)₂Ir(acac) group and compound **12** is nearly as emissive as FIracac in that group. As discussed above, the compounds with CF₃ groups are very weakly emissive, $\Phi \leq 0.02$. This behavior is typically found in compounds with one or more aromatic groups on the β -diketonate ligand such as (F₂ppy)₂Ir(1-phenyl-1,3-butanedionate),⁷² (F₂ppy)₂Ir(avobenzonate),²³ or (F₂ppy)₂Ir(1,3-diphenyl-1,3-propanedionate).⁵⁵ This was also found in a compound with one aromatic and one CF₃ group: (F₂ppy)₂Ir(4,4,4-trifluoro-1-naphthyl-1,3-butanedionate).⁵⁵ In all cases, the low quantum yields were attributed to emission occurring from the triplet state of the ancillary ligand (diketonate) instead of the cyclometallated ligand (F₂ppy). Our TD-DFT results are in accord with this assertion (*vide infra*). The emission lifetimes (τ_{em}) of the molecules in our study are on the microsecond timescale (ave = 1.4 μ sec) typically found for iridium(III) cyclometallates. The complexes with CF₃ groups displayed the fastest nonradiative rate constants, with values in the range of 5.18 - 9.52 $\times 10^5$ s⁻¹.

Table 1. Photophysical properties of the iridium complexes.

Compound	λ_{em} (nm) ^a	Φ_{em} ^b	τ_{em} (μ s)	k_r (10^5 s ⁻¹)	k_{nr} (10^5 s ⁻¹)
1	515, 540	0.54	1.57	3.44	2.93
3	530 (broad)	<0.01	-	-	-
4	513, 540	0.51	1.55	3.29	3.16
5	520, 545	0.74	1.41	5.25	1.84
6	605 (broad)	0.01	1.91	0.05	5.18
8	479, 502	0.74	1.44	5.14	1.81
9	484, 506	0.60	1.15	5.22	3.48
10	506, 540	0.01	1.04	0.10	9.52
11	480, 502	0.55	1.72	3.20	2.62
12	485, 508	0.70	1.14	6.14	2.63
13	610	0.02	1.13	0.18	8.67
14	610	0.01	1.15	0.09	8.61

^aMeasured in 0.1% PMMA discs. ^bRelative to FIrpic with $\Phi = 0.89$;³⁸ values are $\pm 20\%$

TD-DFT Calculations. Time-dependent Kohn-Sham density functional theory calculations (TD-DFT) were performed on the (ppy)₂Ir(acac) series (**1-6**) and FIracac series (**8-14**) in order to gain insight into the electronic structures of the low-lying excited states. Different choices of the exchange-correlation functional under the TD-DFT scheme may result in very distinct excitation energies,⁷³ therefore we compared two different approximations, B3LYP and CAM-B3LYP, to find the most accurate method for our systems. Furthermore, we also benchmarked different choices of the basis set for Ir since the number of basis functions used for the metal may affect the metal-to-ligand excitations. Two basis sets were used for Ir: (i) the Stuttgart/Dresden relativistically corrected effective core potential (ECP) along with a [6s5p3d] valence basis, (ii) the Los Alamos relativistic ECP along with a

[3s3p2d] valence basis. In both cases, the ECPs were used to replace 60 core electrons of iridium. In all cases we used the triple- ζ basis set def2-TZVP for the ligands. Our results (shown in Tables S10 and S11 in the Supporting Information) revealed that B3LYP gave excellent agreement with the measured values and the effect of the iridium basis set choice was negligible. The current results are consistent with our previous TD-DFT calculations on iridium(III) picolinate complexes⁵⁹ as well as with the other benchmark on Ir(III) complexes.⁷⁴ Therefore, the excited states from B3LYP/LANL2DZ (Ir)/def2-TZVP (ligands) will be used in the following discussion.

The six lowest energy singlet (S_1 - S_6) and triplet (T_1 - T_6) transitions are given in Tables S12 (**1, 3-6**) and S13 (**8-14**); the spectroscopically significant singlet excited states are shown in Table 2. Based on oscillator strength calculations, the band found in the 450-460 nm region in the (ppy)₂Iracac series (compounds **1, 3-6**) is assigned to either the $S_0 \rightarrow S_1$ (**1, 3-5**) or $S_0 \rightarrow S_2$ (**6**) transition. The higher energy band near 400 nm in the series corresponds to the $S_0 \rightarrow S_4$ transition, except for compound **4** which has a better fit to $S_0 \rightarrow S_3$. This band cannot be resolved in compound **5** although the oscillator strength suggests $S_0 \rightarrow S_3$ would be the most likely assignment. As mentioned in the spectroscopy discussion above, the band near 495 nm in **1, 3-6** is typically assigned to the lowest energy triplet transition $S_0 \rightarrow T_1$. Our calculations in Table S12 underestimate the energy of this transition by 0.05-0.08 eV. Now, for compounds **8-14** in the FIracac series, oscillator strengths suggest the transition in the 425-440 nm region is assigned to either the $S_0 \rightarrow S_1$ (**8-12**) or $S_0 \rightarrow S_2$ (**12-14**) transition. The higher energy band in the 375-390 nm region may be either the $S_0 \rightarrow S_3$ (**8, 9, 11, 12**), $S_0 \rightarrow S_4$ (**10, 14**), or $S_0 \rightarrow S_5$ (**13**) transition. The weak band near 465 nm for this series is usually assigned as the lowest energy triplet transition $S_0 \rightarrow T_1$ and our calculations are in very good agreement (≤ 0.03 eV) with the observed values except for compounds **13** and **14** which underestimate the experimental energies by 0.24 eV and 0.18 eV, respectively.

Table 2. Comparison of TD-DFT results for low-lying singlet states with experimental data.

Compound	Excited State	$\Delta E_{\text{calc}}(\text{eV})^{\text{a}}$	Osc. Strength (f) ^{a,b}	$\lambda_{\text{calc}}(\text{nm})^{\text{a}}$	$\lambda_{\text{expt}}(\text{nm})^{\text{c}}$
1	S ₁	2.68	0.033	462	460
	S ₄	3.21	0.044	387	410
3	S ₁	2.74	0.034	453	451
	S ₄	3.25	0.010	382	402
4	S ₁	2.69	0.031	461	456
	S ₃	3.08	0.026	402	413
5	S ₁	2.64	0.034	469	462
	S ₃	3.04	0.016	407	-
6	S ₂	2.74	0.032	453	448
	S ₄	3.07	0.017	404	400
8	S ₁	2.90	0.030	427	438
	S ₃	3.30	0.031	376	390
9	S ₁	2.87	0.030	432	440
	S ₃	3.13	0.019	397	394
10	S ₁	2.96	0.031	419	432
	S ₄	3.43	0.034	361	380
11	S ₁	2.91	0.027	427	438
	S ₃	3.16	0.029	392	392
12	S ₁	2.86	0.030	434	438
	S ₃	3.12	0.017	397	394
13	S ₂	3.02	0.032	411	425
	S ₅	3.44	0.053	360	373
14	S ₂	2.96	0.031	418	430
	S ₄	3.17	0.020	391	385

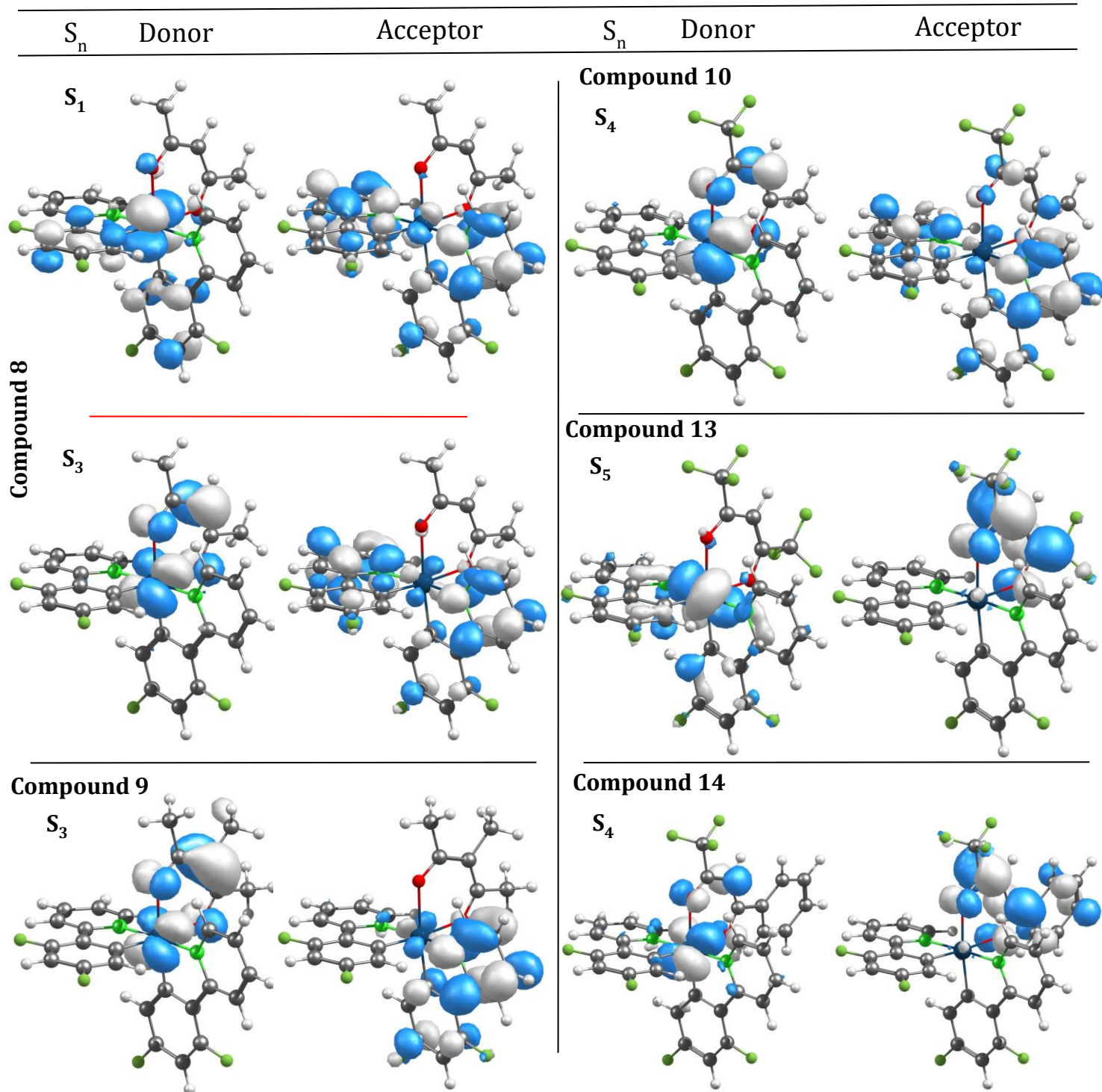
^aValues from Table S12-13 using B3LYP functional with def2-TZVP (ligand)/LANL2DZ (Ir) basis set.

^bOnly singlet states with appreciable oscillator strength are included. ^cMeasured in 0.1% PMMA discs.

We have computed natural transition orbitals (NTOs)⁷⁵ for S₁-S₆ and T₁-T₂ states for all compounds in the FIracac series (**8-14**) and provide full details for these in Tables S14-S28, including the description of the NTOs in terms of molecular orbitals. We also present molecular orbital energy level diagrams and contour plots for complexes **8-14** in Tables S29-36 although we will primarily utilize NTOs in the following discussion. The use of these NTOs provides a simple qualitative description of the electronic transitions for these complexes. NTOs for the lowest energy singlet excited state (S₁) for **8** are given in Table 3 and this serves as the prototype for this transition in all the complexes. We find that the NTOs for this lowest energy singlet band near 435 nm (S₀ → S₁ for **8-12** and S₀ → S₂ for **13-14**) have a very similar appearance for the entire series. Thus, donation from the Ir d-orbital to the phenylpyridine ligands occurs (ML_{ppy}CT) as well as ligand-ligand donation between the phenylpyridine groups (L_{ppy}L_{ppy}CT). There is no involvement of the acetylacetonate ligand in this transition. As shown in Table S14, this lowest energy singlet transition is mainly HOMO → LUMO for **8**, HOMO → LUMO+1 for **10**, **13**, and **14** and a combination of HOMO → LUMO and HOMO → LUMO+1 for **9**, **11**, and **12**. The higher energy singlet transition near 390 nm has more variation in the NTOs and these are shown for representative compounds in Table 3. For all

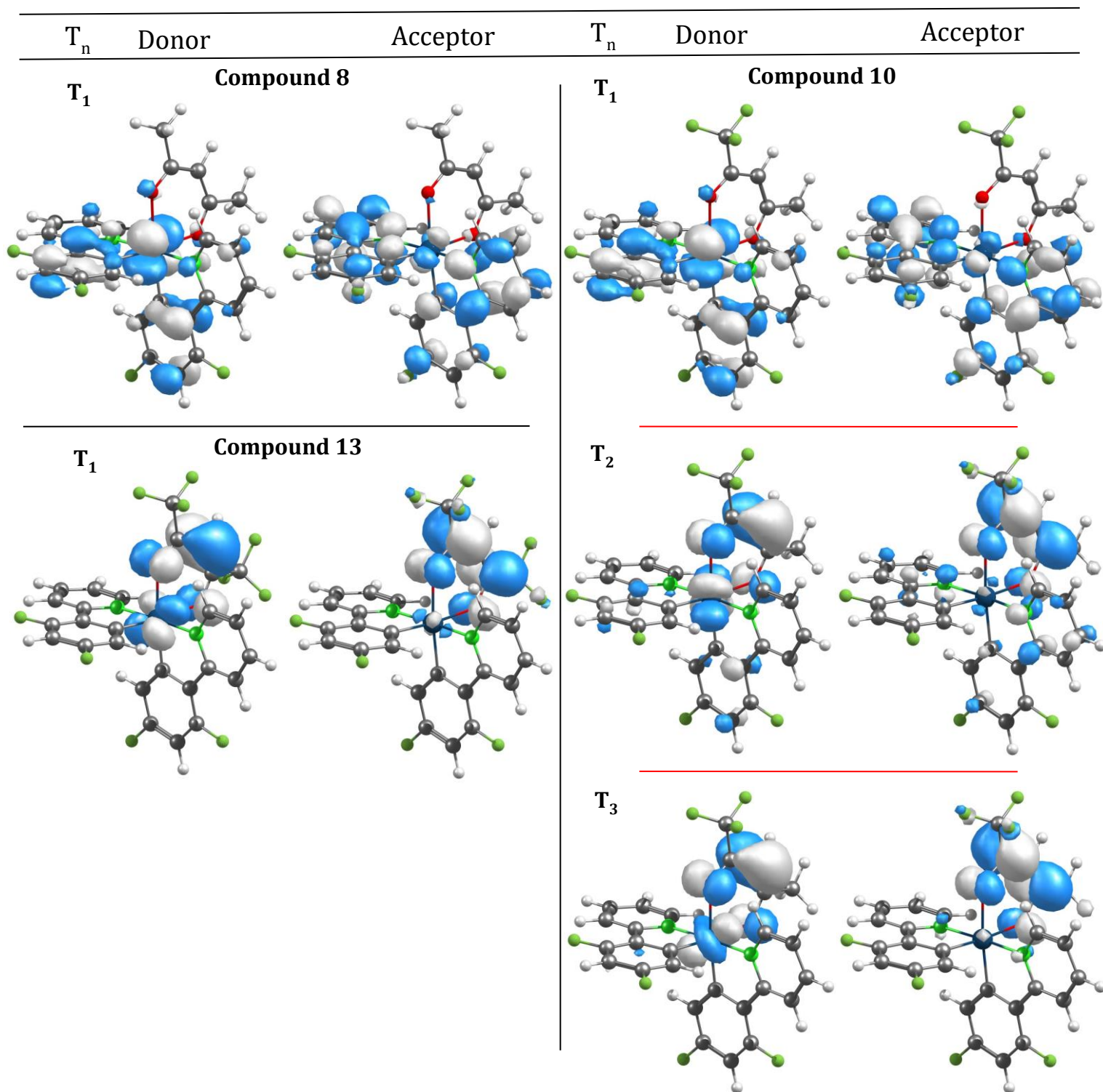
compounds except **13** the donor orbitals have no contribution from the phenylpyridine ligand; the electron density is located on the iridium d-orbital and acetylacetonate ligand. The acceptor orbitals for **8**, **9**, **11**, and **12** involve the phenylpyridine ligands so we can classify the transition on these compounds as $ML_{ppy}CT$ and $L_{acac}L_{ppy}CT$. These are all $S_0 \rightarrow S_3$ transitions. The S_3 NTOs for **8** and **11** are nearly identical so only **8** is shown in Table 3. Similarly, **9** and **12** are nearly identical so only **9** is shown. The acceptor orbital on compound **10** shows predominant involvement of the phenylpyridine group but some small density exists on the acetylacetonate ligand as well; this is the $S_0 \rightarrow S_4$ transition in Table 3. Compound **14** differs from **8-12** since it has acceptor orbital electron density solely on the acetylacetonate ligand (with attached phenyl group) so this transition can be classified as $ML_{acac}CT$ and $L_{acac}L_{acac}CT$. There is no involvement of the phenylpyridine ligand in this $S_0 \rightarrow S_4$ transition. Finally, compound **13** ($S_0 \rightarrow S_5$ transition) has iridium d-orbital and phenylpyridine ligand involvement in its donor NTO while the acceptor orbital is localized on the acetylacetonate ligand. This transition can be classified as $ML_{acac}CT$ and $L_{ppy}L_{acac}CT$. Now, in molecular orbital terms (see Table S14) this approx. 390 nm singlet transition for the FIracac series involves HOMO-1 \rightarrow LUMO (compounds **10** and **14**), HOMO-1 \rightarrow LUMO+1 (compound **8**), and a combination of HOMO-1 \rightarrow LUMO and HOMO-1 \rightarrow LUMO+1 (compounds **9**, **11**, and **12**). Compound **13** is very different, with contributions from HOMO-4 \rightarrow LUMO and HOMO-2 \rightarrow LUMO.

Table 3. Natural transition orbitals (NTOs) for low energy singlet states of **8-10**, and **13-14**.



The NTOs for selected triplet states calculated at the ground state (S_0) geometry are shown in Table 4. Both T_1 and T_2 excited states are considered for **8-12** (T_3 is also included for **10**, see below) since these states are nearly degenerate (≤ 0.03 eV difference) as shown in Table S13. The T_1 and T_2 NTOs for **8, 9, 11**, and **12** are very similar and we provide T_1 for compound **8** as a representative example in Table 4. We find that the low energy triplet transitions for these four compounds incorporate donation from the Ir d-orbital to the phenylpyridine ligands ($ML_{ppy}CT$) as well as ligand-ligand donation between the phenylpyridine groups ($L_{ppy}L_{ppy}CT$). There is no involvement of the acetylacetonate ligand in these transitions. For **8, 9**, and **12** this can be described as $HOMO \rightarrow LUMO$ (T_1) and $HOMO \rightarrow LUMO+1$ (T_2). For **11** each state is a combination of $HOMO \rightarrow LUMO$ and $HOMO \rightarrow LUMO+1$ which differ primarily in the phase of the configuration mixing. Compounds **13** and **14** are also very similar to each other: the T_1 state for **13** is given in Table 4 (the much higher energy T_2 state need not be considered). This $S_0 \rightarrow T_1$ transition comprises donation from the iridium d-orbital to the acetylacetonate ligand ($ML_{acac}CT$) and ligand-ligand donation within the acetylacetonate ($L_{acac}L_{acac}CT$). There is no evidence of involvement of the phenylpyridine ligand in this state. This can be described primarily as $HOMO-1 \rightarrow LUMO$ although **13** also has contributions from $HOMO-6 \rightarrow LUMO$ and $HOMO-3 \rightarrow LUMO$. Finally, compound **10** is set apart in this FIracac series since the three lowest energy triplet states are nearly degenerate ($\Delta E = 2.70, 2.71, \text{ and } 2.72$ eV) with very different NTOs as shown in Table 4. The T_1 state for **10** primarily utilizes phenylpyridine ligands as acceptors so it can be classified as $ML_{ppy}CT$ and $L_{ppy}L_{ppy}CT$. The T_2 state for **10** is unique among the compounds studied here since it involves *both* phenylpyridine and acetylacetonate as acceptor groups and can be viewed as a combination of $ML_{acac}CT$ and $ML_{ppy}CT$. The T_3 state utilizes only the acetylacetonate ligand as an acceptor and is thus $ML_{acac}CT$ and $L_{acac}L_{acac}CT$ in nature. The T_1 state can be described as $HOMO \rightarrow LUMO+1$ while the T_2 and T_3 states comprise $HOMO \rightarrow LUMO$ and $HOMO-1 \rightarrow LUMO+2$ as the main contributors.

Table 4. Natural transition orbitals (NTOs) for low energy triplet states of **8**, **10**, and **13**.



Phosphorescence from cyclometallated iridium complexes is believed to originate from the lowest energy triplet state^{38, 46, 50, 76} so we can use the information culled from the low energy triplet NTOs presented in Table 4 to better understand the emission spectra depicted in Fig. 13. The triplet acceptor orbitals for these complexes can be divided into three types: Type 1 has the acceptor located on the phenylpyridine ligands (compounds **8**, **9**, **11**, and **12**); Type 2 has the acceptor located on the acetylacetonate ligand (compounds **13** and **14**); Type 3 is located on both the acetylacetonate and phenylpyridine ligands (compound **10**, specifically the T₂ state). This treatment has been suggested by Park and coworkers^{60, 76, 77} utilizing molecular orbitals (MOs) for explaining Type 1 and 2 emission. We have chosen to focus on NTOs instead of MOs and also posit Type 3 as a new example.⁵⁹ The Type 1 emission spectra for **8**, **9**, **11**, and **12** are nearly identical with a fairly narrow band containing a longer wavelength shoulder; the emission is greenish blue in color (see Fig. 14 for examples). The Type 2 spectra of **13** and **14** are symmetric and broad with a bathochromic shift giving rise to weak orange emission. Finally, the Type 3 spectrum of **10** has similarities to the Type 1 compounds with a peak at 506 nm and a longer wavelength shoulder. However, it is significantly broadened with a tail extending far into the visible and weak yellow emission.

CONCLUSIONS

We have found that using 1,2-dimethoxyethane as a reaction solvent is superior to the glycol ethers typically employed for ancillary ligand addition to dimeric iridium compounds. For example, acetylacetonate added cleanly to [(F₂ppy)₂IrCl]₂ to form FIracac in refluxing dimethoxyethane under basic conditions. This reaction proceeded quickly in high yield and required no product purification aside from simple filtration and water wash. This is in contrast to the conventional synthesis in 2-ethoxyethanol in which column chromatography is needed to obtain pure material. The ability to omit this purification step becomes even more important with larger scale preparations. We have prepared fifteen cyclometallated Ir(III) acetylacetonates via this route, eight of which are newly reported here. In several instances (compounds **2**, **10**, **13**, and **14**), the use of refluxing 2-ethoxyethanol failed to yield products that were easily obtained with our dimethoxyethane route. X-ray diffraction studies were carried out on nine of the compounds to determine their molecular structures. All the complexes exhibit the same distorted octahedral geometry with two bidentate phenylpyridine ligands and one bidentate acetylacetonate ligand. The iridium-bound nitrogen atoms of the two phenylpyridine ligands are *trans* to each other while the two ligated oxygen atoms in the acetylacetonate ligand are *trans* to the iridium-bound phenyl carbon atoms of the phenylpyridine ligands. The acetylcyclohexanone complexes **5** and **12** display the “half-chair” conformation of the six-membered ring typically found in cyclohexene while the acetylcyclopentanone complex **11** exists in the puckered form common in cyclopentene. The phenyl-substituted acetylacetonates **6** and **14** show the phenyl group rotated out of the diketonate plane by 25° and 34°, respectively.

Seven of the compounds were strongly emissive at room temperature with colors ranging from blue to yellow and quantum yields of 50-75%. All of the complexes containing a trifluoromethyl group (**3**, **6**, **10**, **13**, and **14**) were very weak emitters with $\Phi \leq 0.02$. Measured emission lifetimes for all the compounds were in the range of 1-2 μ s. Time-dependent density functional theory calculations utilizing the B3LYP functional with LANL2DZ (Ir)/def2-TZVP (ligands) basis sets gave close agreement with spectroscopic data. These calculations, visualized with natural transition orbitals for the FIracac series, guided a detailed interpretation of the absorption and emission spectra for the complexes. We found it useful to study the low energy triplet NTOs for the FIracac series to understand the phosphorescence in these complexes. Compounds **8**, **9**, **11**, and **12** have acceptor orbitals located only on the phenylpyridine ligands and are called Type 1 emitters. These display highly efficient greenish blue luminescence with fairly narrow spectral bands. Complexes **13** and **14** have acceptor orbitals involving only the ancillary acetylacetonate ligand and are referred to as Type 2 compounds. These are very inefficient with broad emission bands in the orange region. Finally, compound **10** features acceptor orbitals involving *both* phenylpyridine and acetylacetonate ligands (best illustrated by its T_2 state) and we classify this as Type 3 behavior. This emission spectrum has the general shape of the Type 1 compounds but is broadened appreciably and red-shifted.

EXPERIMENTAL SECTION

General Information. All compounds were synthesized in a dry nitrogen atmosphere, unless otherwise specified. The solvents and commercially available starting materials were of the highest purity available and used as received. Most organic compounds were purchased from TCI America and $\text{IrCl}_3 \cdot x \text{H}_2\text{O}$ was purchased from Strem Chemicals. Silica column chromatography was done with silica gel 60 (particle size 40-63 μ m) from EMD Chemicals. Microanalysis was performed by Galbraith Laboratories, Knoxville, TN. NMR spectra were recorded on a Bruker Avance III 600 MHz spectrometer.

Photophysical and optical spectroscopy measurements. Specimens for absorption and emission measurements were prepared by polymerizing 0.1% solutions of the compounds in methyl methacrylate. This provided 14 mm diam cylinders which were cut and polished to yield ~ 1 mm thick x 14 mm diam discs. Optical absorption spectra were obtained with a Thermo Evolution 220 UV-visible spectrometer. Emission spectra were measured using 425 nm excitation on a Thermo Lumina luminescence spectrometer employing backscatter geometry, excitation and emission slits of 1 mm, a signal averaging time of 0.2 s, and a scan rate of 300 nm/minute. Quantum yields were estimated by sensitivity correcting the emission spectra for the PMT and grating efficiency as a function of wavelength, then normalizing the integrated emission spectra to the optical density of each sample at the excitation wavelength, 425 nm. To estimate the quantum yields of the compounds, their integral light yields were standardized relative to FIrpic (obtained

from American Dye Source), which has a reported value of 0.89 in PMMA.³⁸ Phosphorescence lifetime measurements were acquired using a flashlamp-pumped Nd:YAG laser at 266 nm with 20 ns pulses. Luminescence was collected with a monochromator, set to the emission wavelength maximum for each compound, coupled to an R928 Hamamatsu PMT and read out by an oscilloscope. For each sample, 10 traces were acquired and averaged to generate the decay curves, which were then fit in Igor Pro, for all decays, to single exponentials to obtain the phosphorescence lifetimes.

X-ray crystallography. Suitable crystals for single crystal diffraction studies on compounds **3**, **5**, **6** and **9-14** were obtained by slow evaporation of solvent from dichloromethane/methanol solutions. Single crystal specimens for **3**, **5**, **6**, and **11-14** were collected on a Bruker-AXS VENTURE diffractometer with a MoK α microfocus source ($\lambda = 0.71073 \text{ \AA}$) with a PHOTON-II (CPAD) detector. Unit cell constants were determined initially with APEX3 software.⁷⁸ Single crystal specimens for **9** and **10** were collected on a Bruker-AXS APEX-II CCD diffractometer with a MoK α normal-focus tube source ($\lambda = 0.71073 \text{ \AA}$). Unit cell constants were determined initially with APEX2 software.⁷⁸ Final unit cell constants for all structures were calculated on sets of strong reflections selected from the integration of all data with SAINT.⁷⁸ Multi-scan scaling and absorption correction were applied with SADABS or TWINABS based on the Laue class determined for each crystal structure.⁷⁸ The crystal structures were solved by direct-methods using SHELXT-2014.⁷⁹ Final least-squares refinements were completed with SHELXL-2014.⁸⁰ All non-hydrogen atoms were refined with anisotropic displacements. Hydrogen atoms were placed as riding atoms at calculated positions with isotropic displacements relative to respective host atoms. Specimens **3** and **10** were determined to be twins by non-merohedry. Specimen **12** exhibited whole molecule disorder. Various restraints⁸¹ and constraints were applied to **3**, **5**, **10**, and **12** as detailed in the Supporting Information.

Synthesis. [(ppy)₂IrCl]₂^{53, 54} and [(F₂ppy)₂IrCl]₂^{47, 60} were prepared by the literature methods.

(ppy)₂Ir(acetylacetonate) (Compound 1). A 50 mL round-bottom flask was charged with 1.0 g (9.4 mmol) sodium carbonate and 0.37 g (3.7 mmol) 2,4-pentanedione in 25 ml 1,2-dimethoxyethane. The mixture was purged with nitrogen and 1.0 g (0.93 mmol) [(ppy)₂IrCl]₂ was added. The reaction was brought to reflux and heated for 8 hr under a nitrogen atmosphere. After cooling to room temperature, the reaction was filtered through a glass frit. The solids were washed with three portions of water and three portions of methanol and dried under vacuum to yield 1.0 g of yellow-orange product (89%). ¹H NMR results were identical with those previously reported.⁴²

(ppy)₂Ir(3-methylacetylacetonate) (Compound 2). A 50 mL round-bottom flask was charged with 1.0 g (9.4 mmol) sodium carbonate and 0.43 g (3.7 mmol) 3-methyl-2,4-pentanedione in 25 ml 1,2-dimethoxyethane. The mixture was purged

with nitrogen and 1.0 g (0.93 mmol) [(ppy)₂IrCl]₂ was added. The reaction was brought to reflux and heated for 6 hr under a nitrogen atmosphere. After cooling to room temperature, the reaction was filtered through a glass frit. The solids were washed with three portions of water and three portions of methanol and dried under vacuum to yield 1.0 g of material. NMR analysis revealed equimolar starting material and product and ~4% of unidentified impurity. The reaction was repeated with a 24 hr reflux and similar workup to yield 1.1 g of material. NMR analysis showed no starting material remained, but the impurity seen in the 6 hr reaction was now present at the 25% level. All attempts to obtain analytically pure material were unsuccessful. The NMR spectrum we recorded for compound **2** was somewhat different than that previously reported,⁶¹ specifically in the upfield region displaying the diketonate methyl groups. The prior report found these peaks at 2.17 (3H) and 1.78 (6H) in CDCl₃. Our spectrum shows them at 1.90 (6H) and 1.89 (3H) in excellent agreement with the well-characterized F₂ppy analog **9** (see below) which displays the resonances at 1.92 (s, 6H) and 1.91 (s, 3H). ¹H NMR (600MHz, CDCl₃) (ppm): 8.55 (d, J = 5.5 Hz, 2H), 7.87 (d, J = 8.1 Hz, 2H), 7.74 (t, J = 7.7 Hz, 2H), 7.57 (d, J = 7.7 Hz, 2H), 7.14 (t, J = 6.6 Hz, 2H), 6.81 (t, J = 7.4 Hz, 2H), 6.69 (t, J = 7.4 Hz, 2H), 6.27 (d, J = 7.6 Hz, 2H), 1.90 (s, 6H), 1.89 (s, 3H).

(ppy)₂Ir(1,1,1-trifluoroacetylacetonate) (Compound 3). Procedure as for compound **1**, with 1,1,1-trifluoro-2,4-pentanedione as ligand (76% yield). *Anal.* Calcd for IrC₂₇H₂₀N₂O₂F₃: C, 49.61; H, 3.08; N, 4.29. Found: C, 49.54; H, 2.92; N, 4.20%. ¹H NMR (600MHz, CDCl₃) (ppm): 8.47 (d, J = 5.1 Hz, 1H), 8.41 (d, J = 5.1 Hz, 1H), 7.89 (d, J = 8.3 Hz, 2H), 7.79 (m, 2H), 7.59 (d, J = 7.7 Hz, 1H), 7.56 (d, J = 7.7 Hz, 1H), 7.18 (m, 2H), 6.86 (m, 2H), 6.73 (m, 2H), 6.31 (d, J = 7.0 Hz, 1H), 6.22 (d, J = 7.0 Hz, 1H), 5.62 (s, 1H), 1.90 (s, 3H). ¹⁹F NMR (565 MHz, CDCl₃) (ppm): -74.92 (s, 3F).

(ppy)₂Ir(2-acetylcyclopentanone) (Compound 4). Procedure as for compound **1**, with 2-acetylcyclopentanone as ligand (91% yield). A lower resolution NMR spectrum has been reported;⁶¹ we now report a higher resolution spectrum. ¹H NMR (600MHz, CDCl₃) (ppm): 8.55 (d, J = 5.3 Hz, 1H), 8.50 (d, J = 5.4 Hz, 1H), 7.86 (d, J = 8.1 Hz, 2H), 7.74 (t, J = 7.1 Hz, 2H), 7.56 (t, J = 6.7 Hz, 2H), 7.14 (t, J = 5.8 Hz, 2H), 6.82 (m, 2H), 6.70 (m, 2H), 6.28 (t, J = 7.1 Hz, 2H), 2.67 (t, J = 6.8 Hz, 2H), 2.23 (m, 1H), 2.13 (m, 1H), 1.86 (s, 3H), 1.79 (m, 1H), 1.73 (m, 1H).

(ppy)₂Ir(2-acetylcyclohexanone) (Compound 5). A 50 mL round-bottom flask was charged with 1.0 g (9.4 mmol) sodium carbonate and 0.53 g (3.7 mmol) 2-acetylcyclohexanone in 25 ml 1,2-dimethoxyethane. The mixture was purged with nitrogen and 1.0 g (0.93 mmol) [(ppy)₂IrCl]₂ was added. The reaction was brought to reflux and heated for 6.5 hr under a nitrogen atmosphere. After cooling to room temperature, the reaction was filtered through a glass frit. The solids were washed with three portions of water and three portions of methanol and dried under vacuum to yield 1.0 g of material. NMR analysis revealed a 2:1 ratio of product to starting material. The reaction was repeated with a 24 hr reflux and similar workup to yield 1.1 g of orange-yellow product (92%), with no starting material remaining.

A lower resolution NMR spectrum has been reported;⁶¹ we now report a higher resolution spectrum. ¹H NMR (600MHz, CDCl₃) (ppm): 8.58 (d, J = 5.6 Hz, 1H), 8.55 (d, J = 5.6 Hz, 1H), 7.86 (d, J = 8.1 Hz, 2H), 7.73 (t, J = 7.7 Hz, 2H), 7.56 (t, J = 6.3 Hz, 2H), 7.14 (t, J = 5.8 Hz, 2H), 6.81 (q, J = 7.1 Hz, 2H), 6.69 (q, J = 7.6 Hz, 2H), 6.27 (dd, J = 14.8, 7.6 Hz, 2H), 2.40 (t, J = 5.6 Hz, 2H), 2.09 (m, 1H), 1.95 (m, 1H), 1.86 (s, 3H), 1.62 (m, 2H), 1.60 (m, 1H), 1.57 (m, 1H).

(ppy)₂Ir(4,4,4-trifluoro-1-phenyl-1,3-butanedionate) (Compound 6).

Procedure as for compound **1**, with 4,4,4-trifluoro-1-phenyl-1,3-butanedione as ligand (85% yield). *Anal.* Calcd for IrC₃₂H₂₂N₂O₂F₃: C, 53.70; H, 3.10; N, 3.91.

Found: C, 53.42; H, 3.19; N, 3.67%. ¹H NMR (600MHz, CDCl₃) (ppm): 8.54 (d, J = 5.7 Hz, 1H), 8.44 (d, J = 5.7 Hz, 1H), 7.89 (dd, J = 12.0, 8.1 Hz, 2H), 7.77 (m, 4H), 7.61 (d, J = 7.1 Hz, 1H), 7.59 (d, J = 7.1 Hz, 1H), 7.49 (t, J = 7.4 Hz, 1H), 7.33 (m, 2H), 7.17 (t, J = 7.2 Hz, 1H), 7.11 (t, J = 7.2 Hz, 1H), 6.88 (dt, J = 18.5, 7.0 Hz, 2H), 6.75 (m, 2H), 6.34 (d, J = 7.6 Hz, 1H), 6.33 (s, 1H), 6.29 (d, J = 7.6 Hz, 1H). ¹⁹F NMR (565 MHz, CDCl₃) (ppm): -74.80 (s, 3F).

(ppy)₂Ir(1,3-diphenyl-1,3-propanedionate) (Compound 7). Procedure as for compound **1**, with dibenzoylmethane as ligand (86% yield). ¹H NMR results were identical with those previously reported.⁵⁴

Flracac (Compound 8). A 100 mL round-bottom flask was charged with 1.75 g (16.5 mmol) sodium carbonate and 0.66 g (6.6 mmol) 2,4-pentanedione in 55 ml 1,2-dimethoxyethane. The mixture was purged with nitrogen and 2.00 g (1.64 mmol) [(F₂ppy)₂IrCl]₂ was added. The reaction was brought to reflux and heated for 11 hr under a nitrogen atmosphere. The reaction was then chilled in an ice-water bath prior to filtration through a glass frit. The solids were washed with three portions of water and two portions of ice-cold methanol and dried under vacuum to yield 1.60 g of yellow product (73%). A second batch of product may be obtained by concentrating the original dimethoxyethane filtrate to ~10 mL on a rotovap followed by filtration and washing as above. The combined yield was 1.85 g (84%) of yellow product. NMR spectra taken of both batches were identical. ¹H and ¹⁹F NMR results were in agreement with those previously reported.^{45, 47}

(F₂ppy)₂Ir(3-methylacetylacetonate) (Compound 9). A 50 mL round-bottom flask was charged with 0.87 g (8.2 mmol) sodium carbonate and 0.38 g (3.3 mmol) 3-methyl-2,4-pentanedione in 25 ml 1,2-dimethoxyethane. The mixture was purged with nitrogen and 1.0 g (0.82 mmol) [(F₂ppy)₂IrCl]₂ was added. The reaction was brought to reflux and heated for 6.25 hr under a nitrogen atmosphere. The reaction was then chilled in an ice-water bath prior to filtration through a glass frit. The solids were washed with three portions of water and three portions of ice-cold methanol and dried under vacuum to yield 0.95 g of yellow product (84%). *Anal.* Calcd for IrC₂₈H₂₁N₂O₂F₄: C, 49.05; H, 3.09; N, 4.09. Found: C, 48.76; H, 3.05; N, 4.04%. ¹H NMR (600MHz, CDCl₃) (ppm): 8.48 (d, J = 5.6 Hz, 2H), 8.27 (d, J = 8.3 Hz, 2H), 7.80 (t, J = 7.9 Hz, 2H), 7.19 (d, J = 6.6 Hz, 2H), 6.34 (t, J = 10.9 Hz, 2H), 5.66 (d, J

= 8.9 Hz, 2H), 1.92 (s, 6H), 1.91(s, 3H). ^{19}F NMR (565 MHz, CDCl_3) (ppm): -109.14 (q, J = 9.4 Hz, 2F), -111.25 (t, J = 11.3 Hz, 2F).

(F₂ppy)₂Ir(1,1,1-trifluoroacetylacetonate) (Compound 10). A 50 mL round-bottom flask was charged with 0.87 g (8.2 mmol) sodium carbonate and 0.51 g (3.3 mmol) 1,1,1-trifluoro-2,4-pentanedione in 25 ml 1,2-dimethoxyethane. The mixture was purged with nitrogen and 1.0 g (0.82mmol) [(F₂ppy)₂IrCl]₂ was added. The reaction was brought to reflux and heated for 12 hr under a nitrogen atmosphere. After cooling to room temperature, the reaction was filtered through a glass frit. The solids were washed with two portions of water and two portions of methanol and dried under vacuum to yield 0.37 g of yellow product. Water was added to the original dimethoxyethane filtrate to obtain a second crop of product which was filtered and washed with water and methanol as before. The material was dried under vacuum to obtain an additional 0.69 g of yellow product (combined yield 88%). NMR spectra taken of both fractions were identical. *Anal.* Calcd for IrC₂₇H₁₆N₂O₂F₇: C, 44.69; H, 2.22; N, 3.86. Found: C, 44.23; H, 1.88; N, 3.81%. ^1H NMR (600MHz, CDCl_3) (ppm): 8.40 (d, J = 5.7 Hz, 1H), 8.34 (d, J = 5.7 Hz, 1H), 8.29 (d, J = 8.2 Hz, 2H), 7.86 (t, J = 7.8 Hz, 2H), 7.26 (t, J = 7.2 Hz, 1H), 7.23 (t, J = 7.1 Hz, 1H), 6.40 (t, J = 10.1 Hz, 1H), 6.38 (t, J = 10.1 Hz, 1H), 5.70 (d, J = 8.7 Hz, 1H), 5.67 (s, 1H), 5.61 (d, J = 8.8 Hz, 1H), 1.95 (s, 3H). ^{19}F NMR (565 MHz, CDCl_3) (ppm): -75.03 (s, 3F), -108.32 (q, J = 9.4 Hz, 1F), -108.49 (q, J = 9.4 Hz, 1F), -110.75 (t, J = 11.4 Hz, 1F), -110.82 (t, J = 11.4 Hz, 1F).

(F₂ppy)₂Ir(2-acetylcyclopentanone) (Compound 11). Procedure as for compound **9**, with 2-acetylcyclopentanone as ligand (90% yield). *Anal.* Calcd for IrC₂₉H₂₁N₂O₂F₄: C, 49.92; H, 3.03; N, 4.01. Found: C, 49.81; H, 2.80; N, 3.95%. ^1H NMR (600MHz, CDCl_3) (ppm): 8.48 (d, J = 5.7 Hz, 1H), 8.42 (d, J = 5.7 Hz, 1H), 8.27 (d, J = 8.3 Hz, 2H), 7.81 (t, J = 7.4 Hz, 2H), 7.20 (m, 2H), 6.35 (m, 2H), 5.68 (t, J = 2.7 Hz, 1H), 5.66 (t, J = 2.7 Hz, 1H), 2.68 (t, J = 7.2 Hz, 2H), 2.26 (m, 1H), 2.16 (m, 1H), 1.70-1.85 (m, 2H), 1.88 (s, 3H). ^{19}F NMR (565 MHz, CDCl_3) (ppm): -108.88 (q, J = 9.4 Hz, 1F), -108.90 (q, J = 9.4 Hz, 1F), -111.13 (t, J = 11.5 Hz, 1F), -111.17 (t, J = 11.5 Hz, 1F).

(F₂ppy)₂Ir(2-acetylcyclohexanone) (Compound 12). Procedure as for compound **9**, with 2-acetylcyclohexanone as ligand (85% yield). *Anal.* Calcd for IrC₃₀H₂₃N₂O₂F₄: C, 50.63; H, 3.26; N, 3.94. Found: C, 50.62; H, 3.40; N, 3.90%. ^1H NMR (600MHz, CDCl_3) (ppm): 8.50 (d, J = 5.7 Hz, 1H), 8.47 (d, J = 5.7 Hz, 1H), 8.27 (d, J = 8.1 Hz, 2H), 7.80 (t, J = 7.9 Hz, 2H), 7.19 (m, 2H), 6.34 (m, 2H), 5.67 (dd, J = 8.9, 2.3 Hz, 1H), 5.65 (dd, J = 8.9, 2.3 Hz, 1H), 2.40 (t, J = 5.9 Hz, 2H), 2.12 (m, 1H), 1.97 (m, 1H), 1.89 (s, 3H), 1.60-1.65 (m, 3H), 1.57 (m, 1H). ^{19}F NMR (565 MHz, CDCl_3) (ppm): -109.15 (q, J = 9.5 Hz, 1F), -109.19 (q, J = 9.5 Hz, 1F), -111.25 (t, J = 11.3 Hz, 1F), -111.29 (t, J = 11.3 Hz, 1F).

(F₂ppy)₂Ir(hexafluoroacetonate) (Compound 13). A 50 mL round-bottom flask was charged with 0.87 g (8.2 mmol) sodium carbonate and 0.69 g (3.3 mmol) 1,1,1,5,5,5-hexafluoroacetylacetone in 25 ml 1,2-dimethoxyethane. The mixture was

purged with nitrogen and 1.0 g (0.82 mmol) [(F₂ppy)₂IrCl]₂ was added. The reaction was brought to reflux and heated for 12 hr under a nitrogen atmosphere. After cooling to room temperature, the reaction was filtered through a glass frit. The filtrate was taken to dryness on a rotovap and the solid residue washed twice with water and twice with methanol to yield 0.82 g of orange powder. NMR analysis revealed a 78:22 ratio of product to starting material. The reaction was repeated with a 24 hr reflux and similar workup to yield 1.05 g of material, with only a slightly better ratio of product to starting material (83:17). In addition, a 10% impurity appears that wasn't apparent in the 12 hr reaction. Column chromatography on silica gel using dichloromethane as eluant removed the impurity but did not alter the product:starting material ratio. Soxhlet extraction with hexane was successful in separation of the more soluble product from the insoluble starting material but the recovery was poor after 24 hr (~40%). *Anal.* Calcd for IrC₂₇H₁₃N₂O₂F₁₀: C, 41.60; H, 1.68; N, 3.59. Found: C, 41.52; H, 1.40; N, 3.54%. ¹H NMR (600MHz, CD₂Cl₂) (ppm): 8.35 (d, J = 8.4 Hz, 2H), 8.30 (d, J = 5.6 Hz, 2H), 7.97 (t, J = 7.9 Hz, 2H), 7.35 (t, J = 6.6 Hz, 2H), 6.49 (t, J = 10.7 Hz, 2H), 6.10 (s, 1H), 5.70 (d, J = 8.6 Hz, 2H). ¹⁹F NMR (565 MHz, CDCl₃) (ppm): -75.72 (s, 6F), -107.77 (q, J = 9.4 Hz, 2F), -110.30 (t, J = 11.3 Hz, 2F).

(F₂ppy)₂Ir(4,4,4-trifluoro-1-phenyl-1,3-butanedionate) (Compound 14). A 50 mL round-bottom flask was charged with 0.87 g (8.2 mmol) sodium carbonate and 0.71 g (3.3 mmol) 4,4,4-trifluoro-1-phenyl-1,3-butanedione in 25 ml 1,2-dimethoxyethane. The mixture was purged with nitrogen and 1.0 g (0.82 mmol) [(F₂ppy)₂IrCl]₂ was added. The reaction was brought to reflux and heated for 6 hr under a nitrogen atmosphere. After cooling to room temperature, the reaction was filtered through a glass frit and the filtrate was pumped to dryness on a rotovap. This solid was taken up in 75 mL dichloromethane, transferred to a 125 mL separatory funnel, and extracted with 3 x 30 mL water. The dichloromethane layer was dried over magnesium sulfate and this solution was pumped to dryness on a vacuum line to yield 1.15 g of yellow-orange product (88%). *Anal.* Calcd for IrC₃₂H₁₈N₂O₂F₇: C, 48.79; H, 2.30; N, 3.56. Found: C, 46.21; H, 2.10; N, 3.17%. ¹H NMR (600MHz, CDCl₃) (ppm): 8.48 (d, J = 5.7 Hz, 1H), 8.36 (d, J = 5.7 Hz, 1H), 8.30 (dd, J = 13.6, 8.4 Hz, 2H), 7.84 (dt, J = 11.1, 7.3 Hz, 2H), 7.79 (d, J = 7.3 Hz, 2H), 7.53 (t, J = 7.4 Hz, 1H), 7.37 (t, J = 7.8 Hz, 2H), 7.24 (t, J = 6.2 Hz, 1H), 7.17 (t, J = 6.2 Hz, 1H), 6.42 (m, 2H), 6.36 (s, 1H), 5.75 (dd, J = 2.3, 8.8 Hz, 1H), 5.68 (dd, J = 2.3, 8.8 Hz, 1H). ¹⁹F NMR (565 MHz, CDCl₃) (ppm): -74.89 (s, 3F), -108.51 (q, J = 9.4 Hz, 1F), -108.59 (q, J = 9.4 Hz, 1F), -110.79 (t, J = 11.3 Hz, 1F), -110.95 (t, J = 11.3 Hz, 1F).

(F₂ppy)₂Ir(1,3-diphenyl-1,3-propanedionate) (Compound 15). Procedure as for compound **9**, with dibenzoylmethane as ligand (76% yield). ¹H NMR results were identical with those previously reported.⁵⁵ The ¹⁹F spectrum is reported here for the first time: ¹⁹F NMR (565 MHz, CDCl₃) (ppm): -109.15 (q, J = 9.3 Hz, 2F), -111.31 (t, J = 11.3 Hz, 2F).

TD-DFT Calculations. The ground-state geometries (S₀) of all the complexes were computed by means of Kohn-Sham density functional theory (KS-DFT)⁸²⁻⁸⁴ with

M06-L functional⁸⁵ and the triple- ζ basis set def2-TZVP^{86, 87} for the ligands and the SDD⁸⁸ basis set for Ir. The stationary point characters of the optimized structures were confirmed by the absence of the imaginary modes in the frequency calculations. Time-dependent DFT (TD-DFT)⁸⁹⁻⁹¹ calculations were performed to compute the adiabatic excitations for the S_0 geometries using three different sets of calculation parameters: 1) CAM-B3LYP⁹²/SDD(Ir) /def2-TZVP(Ligand). 2) CAM-B3LYP/LANL2DZ⁹³⁻⁹⁵(Ir)/def2-TZVP(Ligand); 3) B3LYP⁹⁶⁻⁹⁸/LANL2DZ(Ir)/def2-TZVP(Ligand). For each set of calculations, we searched for six low-lying singlet and six low-lying triplet excited states of the iridium(III) complexes. The computed excitation energies together with the experimental measurements are presented in the Supporting Information. The excitations by B3LYP/LANL2DZ(Ir)/def2-TZVP(Ligand) were used to construct the natural transition orbitals (NTOs)⁷⁵ as this method gives an excellent agreement with experiment. The Gaussian 09 (revision D.01) program⁹⁹ was used to carry out all the calculations.

ASSOCIATED CONTENT

Supporting Information

The Supporting Information is available free of charge:

Synthetic procedures (compounds **3**, **4**, **6**, **7**, **11**, **12**, and **15**)

Crystallographic refinement details (compounds **3**, **5**, **10**, and **12**)

X-ray diffraction data and figures (compounds **3**, **5**, **6**, and **9-14**)

UV-Visible spectra

TD-DFT calculations (vertical transition energies for all compounds, natural transition orbitals for **8-14**, molecular orbital energy levels for **8-14**, and molecular orbital contour plots for **8-14**).

¹⁹F spectra (compounds **3**, **6**, and **9-15**) and ¹H NMR spectra (compounds **2-6**, and **9-14**)

Appendix A. Supplementary crystallographic data

The supplementary crystallographic data is available from the CCDC with deposit numbers: 1944851 (**9**), 1944852 (**12**), 1944853 (**11**), 1944854 (**10**), 1944855 (**5**), 1944856 (**13**), 1944857 (**6**), 1944858 (**14**), 1944859 (**3**). These data can be obtained free of charge via <http://www.ccdc.cam.ac.uk/conts/retrieving.html>, or from the Cambridge Crystallographic Data Centre, 12 Union Road, Cambridge CB2 1EZ, UK; fax: (+44) 1223-336-033; or e-mail: deposit@ccdc.cam.ac.uk.

AUTHOR INFORMATION

Corresponding Author

*E-mail: bsanner1@yahoo.com

Notes

The authors declare no competing financial interest.

ACKNOWLEDGMENTS

We would like to thank Prof. Laura Gagliardi (University of Minnesota) for helpful discussions on the quantum chemical calculations. Work at Lawrence Livermore National Laboratory was performed under the auspices of the U.S. DOE under Contract No. DE-AC52-07NA27344 and was supported by the U.S. DOE National Nuclear Security Administration, Defense Nuclear Nonproliferation Research and Development under Contract No. DE-AC03-76SF00098. We thank the X-Ray Crystallographic Laboratory, LeClaire-Dow Instrumentation Facility, Department of Chemistry, University of Minnesota, for its contribution. The authors would like to acknowledge Mr. James T. Moore and the X-Ray Crystallography course CHEM5755 for assistance in collecting single-crystal diffraction data on several complexes presented herein. The Bruker AXS D8 Venture diffractometer was purchased through a grant from NSF/MRI (#1229400) and the University of Minnesota. The computational part of this research (H.P.) was supported by the U.S. Department of Energy, Office of Basic Energy Sciences, Division of Chemical Sciences, Geosciences and Biosciences under Award DE-FG02-17ER16362. The authors acknowledge the Minnesota Supercomputing Institute (MSI) for providing computing resources. LLNL-JRNL-800583

REFERENCES

1. Kim, H.-T.; Seo, J. H.; Ahn, J. H.; Baek, M.-J.; Um, H.-D.; Lee, S.; Roh, D.-H.; Yum, J.-H.; Shin, T. J.; Seo, K.; Kwon, T.-H., Customized Energy Down-Shift Using Iridium Complexes for Enhanced Performance of Polymer Solar Cells. *ACS Energy Letters* **2016**, *1*, 991-999.
2. Sinopoli, A.; Wood, C. J.; Gibson, E. A.; Elliott, P. I. P., New cyclometalated iridium(III) dye chromophore complexes for n-type dye-sensitized solar cells. *Inorganica Chimica Acta* **2017**, *457*, 81-89.
3. Wu, Q. J.; Cheng, Y.; Xue, Z. Y.; Gao, X. Y.; Wang, M. H.; Yuan, W. B.; Huettner, S.; Wan, S. G.; Cao, X. D.; Tao, Y. T.; Huang, W., A cyclometalating organic ligand with an Iridium center toward dramatically improved photovoltaic performance in organic solar cells. *Chemical Communications* **2019**, *55*, 2640-2643.
4. Fleetham, T. B.; Wang, Z.; Li, J., Exploring Cyclometalated Ir Complexes as Donor Materials for Organic Solar Cells. *Inorganic Chemistry* **2013**, *52*, 7338-7343.
5. Gennari, M.; Légalité, F.; Zhang, L.; Pellegrin, Y.; Blart, E.; Fortage, J.; Brown, A. M.; Deronzier, A.; Collomb, M.-N.; Boujtita, M.; Jacquemin, D.; Hammarström, L.; Odobel, F., Long-Lived Charge Separated State in NiO-Based p-Type Dye-Sensitized Solar Cells with Simple Cyclometalated Iridium Complexes. *The Journal of Physical Chemistry Letters* **2014**, *5*, 2254-2258.
6. Tan, G.; Liu, P.; Wu, H.; Yiu, S.-C.; Dai, F.; Feng, Y.-H.; Liu, X.; Qiu, Y.; Lo, Y. H.; Ho, C.-L.; Wong, W.-Y., New iridium(III) cyclometalates with extended absorption features for bulk heterojunction solar cells. *Journal of Organometallic Chemistry* **2016**, *812*, 280-286.
7. Marín-Suárez, M.; Curchod, B. F. E.; Tavernelli, I.; Rothlisberger, U.; Scopelliti, R.; Jung, I.; Di Censo, D.; Grätzel, M.; Fernández-Sánchez, J. F.; Fernández-Gutiérrez,

- A.; Nazeeruddin, M. K.; Baranoff, E., Nanocomposites Containing Neutral Blue Emitting Cyclometalated Iridium(III) Emitters for Oxygen Sensing. *Chemistry of Materials* **2012**, *24*, 2330-2338.
8. Yang, X. L.; Feng, Z.; Dang, J. S.; Sun, Y. H.; Zhou, G. J.; Wong, W. Y., High performance solution-processed organic yellow light-emitting devices and fluoride ion sensors based on a versatile phosphorescent Ir(III) complex. *Materials Chemistry Frontiers* **2019**, *3*, 376-384.
9. Xie, Z.; Ma, L.; deKrafft, K. E.; Jin, A.; Lin, W., Porous Phosphorescent Coordination Polymers for Oxygen Sensing. *Journal of the American Chemical Society* **2010**, *132*, 922-923.
10. Fischer Lorenz, H.; Stich Matthias, I. J.; Wolfbeis Otto, S.; Tian, N.; Holder, E.; Schäferling, M., Red- and Green-Emitting Iridium(III) Complexes for a Dual Barometric and Temperature-Sensitive Paint. *Chemistry – A European Journal* **2009**, *15*, 10857-10863.
11. Zhang, K. Y.; Liu, H.-W.; Tang, M.-C.; Choi, A. W.-T.; Zhu, N.; Wei, X.-G.; Lau, K.-C.; Lo, K. K.-W., Dual-Emissive Cyclometalated Iridium(III) Polypyridine Complexes as Ratiometric Biological Probes and Organelle-Selective Bioimaging Reagents. *Inorganic Chemistry* **2015**, *54*, 6582-6593.
12. Sansee, A.; Meksawangwong, S.; Chainok, K.; Franz, K. J.; Gal, M.; Palsson, L. O.; Puniyan, W.; Traiphol, R.; Pal, R.; Kielar, F., Novel aminoalkyl tris-cyclometalated iridium complexes as cellular stains. *Dalton Transactions* **2016**, *45*, 17420-17430.
13. Zhang, K. Y.; Zhang, T. W.; Wei, H. J.; Wu, Q.; Liu, S. J.; Zhao, Q.; Huang, W., Phosphorescent iridium(III) complexes capable of imaging and distinguishing between exogenous and endogenous analytes in living cells. *Chemical Science* **2018**, *9*, 7236-7240.
14. Campbell, I. H.; Crone, B. K., Efficient plastic scintillators utilizing phosphorescent dopants. *Applied Physics Letters* **2007**, *90*, 012117.
15. Osakada, Y.; Prax, G.; Hanson, L.; Solomon, P. E.; Xing, L.; Cui, B. X., X-ray excitable luminescent polymer dots doped with an iridium(III) complex. *Chemical Communications* **2013**, *49*, 4319-4321.
16. Bertrand, G. H. V.; Hamel, M.; Normand, S.; Sguerra, F., Pulse shape discrimination between (fast or thermal) neutrons and gamma rays with plastic scintillators: State of the art. *Nuclear Instruments and Methods in Physics Research Section A: Accelerators, Spectrometers, Detectors and Associated Equipment* **2015**, *776*, 114-128.
17. Rupert, B. L.; Cherepy, N. J.; Sturm, B. W.; Sanner, R. D.; Payne, S. A., Bismuth-loaded plastic scintillators for gamma-ray spectroscopy. *EPL (Europhysics Letters)* **2012**, *97*, 22002.
18. Sguerra, F.; Marion, R.; Bertrand, G. H. V.; Coulon, R.; Sauvageot, E.; Daniellou, R.; Renaud, J. L.; Gaillard, S.; Hamel, M., Thermo- and radioluminescent polystyrene based plastic scintillators doped with phosphorescent iridium(III) complexes. *Journal of Materials Chemistry C* **2014**, *2*, 6125-6133.
19. Henwood, A. F.; Pal, A. K.; Cordes, D. B.; Slawin, A. M. Z.; Rees, T. W.; Momblona, C.; Babaei, A.; Pertegas, A.; Orti, E.; Bolink, H. J.; Baranoff, E.; Zysman-Colman, E., Blue-emitting cationic iridium(III) complexes featuring

pyridylpyrimidine ligands and their use in sky-blue electroluminescent devices.

Journal of Materials Chemistry C **2017**, *5*, 9638-9650.

20. Namanga, J. E.; Gerlitzki, N.; Smetana, V.; Mudring, A. V., Supramolecularly Caged Green-Emitting Ionic Ir(III)-Based Complex with Fluorinated CN Ligands and Its Application in Light-Emitting Electrochemical Cells. *Acs Applied Materials & Interfaces* **2018**, *10*, 11026-11036.
21. Di Marcantonio, M.; Namanga, J. E.; Smetana, V.; Gerlitzki, N.; Vollkommer, F.; Mudring, A. V.; Bacher, G.; Nannen, E., Green-yellow emitting hybrid light emitting electrochemical cell. *Journal of Materials Chemistry C* **2017**, *5*, 12062-12068.
22. Housecroft, C. E.; Constable, E. C., Over the LEC rainbow: Colour and stability tuning of cyclometallated iridium(III) complexes in light-emitting electrochemical cells. *Coordination Chemistry Reviews* **2017**, *350*, 155-177.
23. Zhou, Y.; Gao, H.; Wang, X.; Qi, H., Electrogenerated Chemiluminescence from Heteroleptic Iridium(III) Complexes with Multicolor Emission. *Inorganic Chemistry* **2015**, *54*, 1446-1453.
24. Park, J.; Kim, T.; Kim, H. J.; Hong, J. I., Iridium(III) complex-based electrochemiluminescent probe for H₂S. *Dalton Transactions* **2019**, *48*, 4565-4573.
25. Fang, Y. Y.; Wang, Z. Y.; Li, Y.; Quan, Y. W.; Cheng, Y. X., The amplified electrochemiluminescence response signal promoted by the Ir(III)-containing polymer complex. *Analyst* **2018**, *143*, 2405-2410.
26. Han, D. J.; Qian, M. P.; Gao, H. F.; Wang, B.; Qi, H. L.; Zhang, C. X., A "switch-on" photoluminescent and electrochemiluminescent multisignal probe for hypochlorite via a cyclometalated iridium complex. *Analytica Chimica Acta* **2019**, *1074*, 98-107.
27. Chi, Y.; Chou, P.-T., Transition-metal phosphors with cyclometalating ligands: fundamentals and applications. *Chemical Society Reviews* **2010**, *39*, 638-655.
28. Xu, F.; Kim, H. U.; Kim, J. H.; Jung, B. J.; Grimsdale, A. C.; Hwang, D. H., Progress and perspective of iridium-containing phosphorescent polymers for light-emitting diodes. *Progress in Polymer Science* **2015**, *47*, 92-121.
29. Zanoni, K. P. S.; Coppo, R. L.; Amaral, R. C.; Iha, N. Y. M., Ir(III) complexes designed for light-emitting devices: beyond the luminescence color array. *Dalton Transactions* **2015**, *44*, 14559-14573.
30. Niu, Z. G.; Han, H. B.; Li, M.; Zhao, Z.; Chen, G. Y.; Zheng, Y. X.; Li, G. N.; Zuo, J. L., Tunable Emission Color of Iridium(III) Complexes with Phenylpyrazole Derivatives as the Main Ligands for Organic Light Emitting Diodes. *Organometallics* **2018**, *37*, 3154-3164.
31. Ho, C.-L.; Wong, W.-Y., Small-molecular blue phosphorescent dyes for organic light-emitting devices. *New Journal of Chemistry* **2013**, *37*, 1665-1683.
32. Gonzalez, I.; Cortes-Arriagada, D.; Dreyse, P.; Sanhueza-Vega, L.; Ledoux-Rak, I.; Andrade, D.; Brito, I.; Toro-Labbe, A.; Soto-Arriaza, M.; Caramori, S.; Loeb, B., A Family of Ir-III Complexes with High Nonlinear Optical Response and Their Potential Use in Light-Emitting Devices. *European Journal of Inorganic Chemistry* **2015**, 4946-4955.
33. Liao, J. L.; Rajakannu, P.; Gnanasekaran, P.; Tsai, S. R.; Lin, C. H.; Liu, S. H.; Chang, C. H.; Lee, G. H.; Chou, P. T.; Chen, Z. N.; Chi, Y., Luminescent Diiridium Complexes with Bridging Pyrazolates: Characterization and Fabrication of OLEDs Using Vacuum Thermal Deposition. *Advanced Optical Materials* **2018**, *6*, 12.

34. Jang, J. H.; Park, H. J.; Park, J. Y.; Kim, H. U.; Hwang, D. H., Orange phosphorescent Ir(III) complexes consisting of substituted 2-phenylbenzothiazole for solution-processed organic light-emitting diodes. *Organic Electronics* **2018**, *60*, 31-37.
35. Grzelak, I.; Orwat, B.; Kownacki, I.; Hoffmann, M., Quantum-chemical studies of homoleptic iridium(III) complexes in OLEDs: fac versus mer isomers. *Journal of Molecular Modeling* **2019**, *25*, 9.
36. Baranoff, E.; Yum, J.-H.; Graetzel, M.; Nazeeruddin, M. K., Cyclometallated iridium complexes for conversion of light into electricity and electricity into light. *Journal of Organometallic Chemistry* **2009**, *694*, 2661-2670.
37. Baldo, M. A.; Thompson, M. E.; Forrest, S. R., High-efficiency fluorescent organic light-emitting devices using a phosphorescent sensitizer. *Nature* **2000**, *403*, 750.
38. Rausch, A. F.; Thompson, M. E.; Yersin, H., Blue Light Emitting Ir(III) Compounds for OLEDs - New Insights into Ancillary Ligand Effects on the Emitting Triplet State. *The Journal of Physical Chemistry A* **2009**, *113*, 5927-5932.
39. Reddy, M. L. P.; Bejoomohandas, K. S., Evolution of 2, 3'-bipyridine class of cyclometalating ligands as efficient phosphorescent iridium(III) emitters for applications in organic light emitting diodes. *Journal of Photochemistry and Photobiology C-Photochemistry Reviews* **2016**, *29*, 29-47.
40. Smith, A. R. G.; Burn, P. L.; Powell, B. J., Spin-Orbit Coupling in Phosphorescent Iridium(III) Complexes. *ChemPhysChem* **2011**, *12*, 2429-2438.
41. Adachi, C.; Baldo, M. A.; Thompson, M. E.; Forrest, S. R., Nearly 100% internal phosphorescence efficiency in an organic light-emitting device. *Journal of Applied Physics* **2001**, *90*, 5048-5051.
42. Lamansky, S.; Djurovich, P.; Murphy, D.; Abdel-Razzaq, F.; Kwong, R.; Tsyba, I.; Bortz, M.; Mui, B.; Bau, R.; Thompson, M. E., Synthesis and Characterization of Phosphorescent Cyclometalated Iridium Complexes. *Inorganic Chemistry* **2001**, *40*, 1704-1711.
43. Tamayo, A. B.; Alleyne, B. D.; Djurovich, P. I.; Lamansky, S.; Tsyba, I.; Ho, N. N.; Bau, R.; Thompson, M. E., Synthesis and Characterization of Facial and Meridional Tris-cyclometalated Iridium(III) Complexes. *Journal of the American Chemical Society* **2003**, *125*, 7377-7387.
44. Adachi, C.; Kwong, R. C.; Djurovich, P.; Adamovich, V.; Baldo, M. A.; Thompson, M. E.; Forrest, S. R., Endothermic energy transfer: A mechanism for generating very efficient high-energy phosphorescent emission in organic materials. *Applied Physics Letters* **2001**, *79*, 2082-2084.
45. Baranoff, E.; Curchod, B. F. E.; Frey, J.; Scopelliti, R.; Kessler, F.; Tavernelli, I.; Rothlisberger, U.; Grätzel, M.; Nazeeruddin, M. K., Acid-Induced Degradation of Phosphorescent Dopants for OLEDs and Its Application to the Synthesis of Tris-heteroleptic Iridium(III) Bis-cyclometalated Complexes. *Inorganic Chemistry* **2012**, *51*, 215-224.
46. Baranoff, E.; Curchod, B. F. E., Irpic: archetypal blue phosphorescent emitter for electroluminescence. *Dalton Transactions* **2015**, *44*, 8318-8329.

47. Li, J.; Djurovich, P. I.; Alleyne, B. D.; Tsyba, I.; Ho, N. N.; Bau, R.; Thompson, M. E., Synthesis and characterization of cyclometalated Ir(III) complexes with pyrazolyl ancillary ligands. *Polyhedron* **2004**, *23*, 419-428.
48. Park, N. G.; Choi, G. C.; Lee, Y. H.; Kim, Y. S., Theoretical studies on the ground and excited states of blue phosphorescent cyclometalated Ir(III) complexes having ancillary ligand. *Current Applied Physics* **2006**, *6*, 620-626.
49. Li, H.; Winget, P.; Risko, C.; Sears, J. S.; Bredas, J.-L., Tuning the electronic and photophysical properties of heteroleptic iridium(III) phosphorescent emitters through ancillary ligand substitution: a theoretical perspective. *Physical Chemistry Chemical Physics* **2013**, *15*, 6293-6302.
50. Gu, X.; Fei, T.; Zhang, H.; Xu, H.; Yang, B.; Ma, Y.; Liu, X., Theoretical Studies of Blue-Emitting Iridium Complexes with Different Ancillary Ligands. *The Journal of Physical Chemistry A* **2008**, *112*, 8387-8393.
51. Hay, P. J., Theoretical Studies of the Ground and Excited Electronic States in Cyclometalated Phenylpyridine Ir(III) Complexes Using Density Functional Theory. *The Journal of Physical Chemistry A* **2002**, *106*, 1634-1641.
52. Nonoyama, M., Benzo[h]quinolin-10-yl-N Iridium(III) Complexes. *Bulletin of the Chemical Society of Japan* **1974**, *47*, 767-768.
53. Sprouse, S.; King, K. A.; Spellane, P. J.; Watts, R. J., Photophysical effects of metal-carbon sigma bonds in ortho-metalated complexes of iridium(III) and rhodium(III). *Journal of the American Chemical Society* **1984**, *106*, 6647-6653.
54. Lamansky, S.; Djurovich, P.; Murphy, D.; Abdel-Razzaq, F.; Lee, H.-E.; Adachi, C.; Burrows, P. E.; Forrest, S. R.; Thompson, M. E., Highly Phosphorescent Bis-Cyclometalated Iridium Complexes: Synthesis, Photophysical Characterization, and Use in Organic Light Emitting Diodes. *Journal of the American Chemical Society* **2001**, *123*, 4304-4312.
55. Gu, X.; Fei, T.; Zhang, H.; Xu, H.; Yang, B.; Ma, Y.; Liu, X., Tuning the Emission Color of Iridium(III) Complexes with Ancillary Ligands: A Combined Experimental and Theoretical Study. *European Journal of Inorganic Chemistry* **2009**, *2009*, 2407-2414.
56. Liu, Z.; Bian, Z.; Hao, F.; Nie, D.; Ding, F.; Chen, Z.; Huang, C., Highly efficient, orange-red organic light-emitting diodes using a series of green-emission iridium complexes as hosts. *Organic Electronics* **2009**, *10*, 247-255.
57. Cherepy, N. J.; Sanner, R. D.; Beck, P. R.; Swanberg, E. L.; Tillotson, T. M.; Payne, S. A.; Hurlbut, C. R., Bismuth- and lithium-loaded plastic scintillators for gamma and neutron detection. *Nuclear Instruments and Methods in Physics Research Section A: Accelerators, Spectrometers, Detectors and Associated Equipment* **2015**, *778*, 126-132.
58. Sanner, R. D.; Cherepy, N. J.; Young, V. G., Blue light emission from cyclometalated iridium(III) cyano complexes: Syntheses, crystal structures, and photophysical properties. *Inorganica Chimica Acta* **2016**, *440*, 165-171.
59. Sanner, R. D.; Cherepy, N. J.; Martinez, H. P.; Pham, H. Q.; Young, V. G., Highly efficient phosphorescence from cyclometalated iridium(III) compounds: Improved syntheses of picolinate complexes and quantum chemical studies of their electronic structures. *Inorganica Chimica Acta* **2019**, DOI: 10.1016/j.ica.2019.119040.

60. You, Y.; Park, S. Y., Inter-Ligand Energy Transfer and Related Emission Change in the Cyclometalated Heteroleptic Iridium Complex: Facile and Efficient Color Tuning over the Whole Visible Range by the Ancillary Ligand Structure. *Journal of the American Chemical Society* **2005**, *127*, 12438-12439.
61. Kim, D.-U.; Paik, S.-H.; Kim, S.-H.; Tak, Y.-H.; Han, Y.-S.; Kim, S.-D.; Kim, K.-D.; Ju, H.-J.; Moon, H.-W.; Kim, T.-J., Novel Green Phosphorescent Materials with Various Substituted Acetylacetonate Ligands for Organic Electroluminescent Device. *Molecular Crystals and Liquid Crystals* **2004**, *424*, 111-117.
62. Dumur, F.; Lepeltier, M.; Siboni, H. Z.; Gimes, D.; Aziz, H., Phosphorescent organic light-emitting devices (PhOLEDs) based on heteroleptic bis-cyclometalated complexes using acetylacetonate as the ancillary ligand. *Synthetic Metals* **2014**, *198*, 131-136.
63. Kim, D. U.; Paik, S.-H.; Kim, S.-H.; Tak, Y.-H.; Kim, S.-D.; Kim, K.-D.; Ju, H.-J.; Kim, T.-J.; Baek, J.-J.; Jeong, Y. C.; Park, L. S.; Han, Y. S., Iridium Complexes With 3-Methyl-2,4-Pentanedione Ligand For Organic Electroluminescent Device. *Journal of Nonlinear Optical Physics & Materials* **2005**, *14*, 529-534.
64. Shin, C. H.; Huh, J. O.; Lee, M. H.; Do, Y., Polymorphism-induced dual phosphorescent emission from solid-state iridium(III) complex. *Dalton Transactions* **2009**, 6476-6479.
65. Groom Colin, R.; Bruno Ian, J.; Lightfoot Matthew, P.; Ward Suzanna, C., The Cambridge Structural Database. *Acta Crystallographica Section B* **2016**, *72*, 171-179.
66. Beckett, C. W.; Freeman, N. K.; Pitzer, K. S., The Thermodynamic Properties and Molecular Structure of Cyclopentene and Cyclohexene1. *Journal of the American Chemical Society* **1948**, *70*, 4227-4230.
67. Jensen, F. R.; Bushweller, C. H., Conformational preferences and interconversion barriers in cyclohexene and derivatives. *Journal of the American Chemical Society* **1969**, *91*, 5774-5782.
68. Kim, T.-J.; Lee, U., cis-(3-Methyl-pentane-2,4-dionato- κ 2O,O')bis-(2-phenyl-pyridine- κ 2C,N)iridium(III). *Acta Crystallographica Section E* **2006**, *62*, m2244-m2245.
69. Pasternak, R. A., The Crystal Structure of a Pentachlorocyclohexene, C₆H₅Cl₅. *Acta Crystallographica* **1951**, *4*, 316-319.
70. Kim, T.-J.; Lee, U., cis-(2-Acetyl-cyclo-penta-nonato- κ 2O,O')bis-(2-pyridylphen-yl- κ N)iridium(III) dichloro-methane solvate. *Acta Crystallographica Section E* **2006**, *62*, m2403-m2405.
71. Frey, J.; Curchod, B. F. E.; Scopelliti, R.; Tavernelli, I.; Rothlisberger, U.; Nazeeruddin, M. K.; Baranoff, E., Structure-property relationships based on Hammett constants in cyclometalated iridium(III) complexes: their application to the design of a fluorine-free FIrPic-like emitter. *Dalton Transactions* **2014**, *43*, 5667-5679.
72. Huang, K.; Wu, H.; Shi, M.; Li, F.; Yi, T.; Huang, C., Reply to comment on 'aggregation-induced phosphorescent emission (AIPE) of iridium(III) complexes': origin of the enhanced phosphorescence. *Chemical Communications* **2009**, 1243-1245.
73. Guido, C. A.; Knecht, S.; Kongsted, J.; Mennucci, B., Benchmarking Time-Dependent Density Functional Theory for Excited State Geometries of Organic

- Molecules in Gas-Phase and in Solution. *Journal of Chemical Theory and Computation* **2013**, *9*, 2209-2220.
74. Latouche, C.; Skouteris, D.; Palazzetti, F.; Barone, V., TD-DFT Benchmark on Inorganic Pt(II) and Ir(III) Complexes. *Journal of Chemical Theory and Computation* **2015**, *11*, 3281-3289.
75. Martin, R. L., Natural transition orbitals. *The Journal of Chemical Physics* **2003**, *118*, 4775-4777.
76. You, Y.; Park, S. Y., Phosphorescent iridium(iii) complexes: toward high phosphorescence quantum efficiency through ligand control. *Dalton Transactions* **2009**, 1267-1282.
77. Seo, J.; Kim, S.; Park, S. Y., Strong Solvatochromic Fluorescence from the Intramolecular Charge-Transfer State Created by Excited-State Intramolecular Proton Transfer. *Journal of the American Chemical Society* **2004**, *126*, 11154-11155.
78. Bruker, *APEX2, APEX3, SAINT, SADABS, and TWINABS*. Bruker AXS Inc.: Madison, Wisconsin, USA, 2015.
79. Sheldrick, G. M., SHELXT- Integrated space-group and crystal-structure determination. *Acta Crystallographica Section A* **2015**, *71*, 3-8.
80. Sheldrick, G., Crystal structure refinement with SHELXL. *Acta Crystallographica Section C* **2015**, *71*, 3-8.
81. Thorn, A.; Dittrich, B.; Sheldrick, G. M., Enhanced rigid-bond restraints. *Acta Crystallographica Section A* **2012**, *68*, 448-451.
82. Hohenberg, P.; Kohn, W., Inhomogeneous Electron Gas. *Physical Review* **1964**, *136*, B864-B871.
83. Kohn, W.; Sham, L. J., Self-Consistent Equations Including Exchange and Correlation Effects. *Physical Review* **1965**, *140*, A1133-A1138.
84. Levy, M., Universal variational functionals of electron densities, first-order density matrices, and natural spin-orbitals and solution of the $\langle v \rangle$ -representability problem. *Proceedings of the National Academy of Sciences* **1979**, *76*, 6062.
85. Zhao, Y.; Truhlar, D. G., A new local density functional for main-group thermochemistry, transition metal bonding, thermochemical kinetics, and noncovalent interactions. *The Journal of Chemical Physics* **2006**, *125*, 194101.
86. Weigend, F., Accurate Coulomb-fitting basis sets for H to Rn. *Physical Chemistry Chemical Physics* **2006**, *8*, 1057-1065.
87. Weigend, F.; Ahlrichs, R., Balanced basis sets of split valence, triple zeta valence and quadruple zeta valence quality for H to Rn: Design and assessment of accuracy. *Physical Chemistry Chemical Physics* **2005**, *7*, 3297-3305.
88. Dolg, M.; Wedig, U.; Stoll, H.; Preuss, H., Energy-adjusted ab initio pseudopotentials for the first row transition elements. *The Journal of Chemical Physics* **1987**, *86*, 866-872.
89. Runge, E.; Gross, E. K. U., Density-Functional Theory for Time-Dependent Systems. *Physical Review Letters* **1984**, *52*, 997-1000.
90. Adamo, C.; Jacquemin, D., The calculations of excited-state properties with Time-Dependent Density Functional Theory. *Chemical Society Reviews* **2013**, *42*, 845-856.

91. Stratmann, R. E.; Scuseria, G. E.; Frisch, M. J., An efficient implementation of time-dependent density-functional theory for the calculation of excitation energies of large molecules. *The Journal of Chemical Physics* **1998**, *109*, 8218-8224.
92. Yanai, T.; Tew, D. P.; Handy, N. C., A new hybrid exchange–correlation functional using the Coulomb-attenuating method (CAM-B3LYP). *Chemical Physics Letters* **2004**, *393*, 51-57.
93. Wadt, W. R.; Hay, P. J., Ab initio effective core potentials for molecular calculations. Potentials for main group elements Na to Bi. *The Journal of Chemical Physics* **1985**, *82*, 284-298.
94. Hay, P. J.; Wadt, W. R., Ab initio effective core potentials for molecular calculations. Potentials for K to Au including the outermost core orbitals. *The Journal of Chemical Physics* **1985**, *82*, 299-310.
95. Hay, P. J.; Wadt, W. R., Ab initio effective core potentials for molecular calculations. Potentials for the transition metal atoms Sc to Hg. *The Journal of Chemical Physics* **1985**, *82*, 270-283.
96. Stephens, P. J.; Devlin, F. J.; Chabalowski, C. F.; Frisch, M. J., Ab Initio Calculation of Vibrational Absorption and Circular Dichroism Spectra Using Density Functional Force Fields. *The Journal of Physical Chemistry* **1994**, *98*, 11623-11627.
97. Becke, A. D., Density-functional thermochemistry. III. The role of exact exchange. *The Journal of Chemical Physics* **1993**, *98*, 5648-5652.
98. Lee, C.; Yang, W.; Parr, R. G., Development of the Colle-Salvetti correlation-energy formula into a functional of the electron density. *Physical Review B* **1988**, *37*, 785-789.
99. Frisch, M. J.; Trucks, G. W.; Schlegel, H. B.; Scuseria, G. E.; Robb, M. A.; Cheeseman, J. R.; Scalmani, G.; Barone, V.; Mennucci, B.; Petersson, G. A.; Nakatsuji, H.; Caricato, M.; Li, X.; Hratchian, H. P.; Izmaylov, A. F.; Bloino, J.; Zheng, G.; Sonnenberg, J. L.; Hada, M.; Ehara, M.; Toyota, K.; Fukuda, R.; Hasegawa, J.; Ishida, M.; Nakajima, T.; Honda, Y.; Kitao, O.; Nakai, H.; Vreven, T.; Montgomery, J. A.; Peralta, J. E.; Ogliaro, F.; Bearpark, M.; Heyd, J. J.; Brothers, E.; Kudin, K. N.; Staroverov, V. N.; Kobayashi, R.; Normand, J.; Raghavachari, K.; Rendell, A.; Burant, J. C.; Iyengar, S. S.; Tomasi, J.; Cossi, M.; Rega, N.; Millam, J. M.; Klene, M.; Knox, J. E.; Cross, J. B.; Bakken, V.; Adamo, C.; Jaramillo, J.; Gomperts, R.; Stratmann, R. E.; Yazyev, O.; Austin, A. J.; Cammi, R.; Pomelli, C.; Ochterski, J. W.; Martin, R. L.; Morokuma, K.; Zakrzewski, V. G.; Voth, G. A.; Salvador, P.; Dannenberg, J. J.; Dapprich, S.; Daniels, A. D.; Farkas, Foresman, J. B.; Ortiz, J. V.; Cioslowski, J.; Fox, D. J., Gaussian 09, Revision D.01. Wallingford CT, 2009.